Stony Brook University

Carbon Nanotubes as Localized Microwave Hyperthermia Agents

A Dissertation Presented

by

Shawn X. Xie

to

The Graduate School

in Partial Fulfillment of the

Requirements

for the Degree of

Doctor of Philosophy

in

Biomedical Engineering

Stony Brook University

August 2016

Stony Brook University

The Graduate School

Shawn X. Xie

We, the dissertation committee for the above candidate for the

Doctor of Philosophy degree, hereby recommend

acceptance of this dissertation

Dr. Balaji Sitharaman – Dissertation Advisor
Associate Professor
Department of Biomedical Engineering

Dr. Paul Vaska – Chairperson of Defense
Professor
Department of Biomedical Engineering and Radiology

Dr. Terry Button
Associate Professor of Radiology and Biomedical Engineering

Dr. Susan C. Hagness
Philip Dunham Reed Professor
Department of Electrical and Computer Engineering
University of Wisconsin-Madison

This dissertation is accepted by the Graduate School

Nancy Goroff

Interim Dean of the Graduate School

ii

Abstract of the Dissertation

Carbon Nanotubes as Localized Microwave Hyperthermia Agents

by

Shawn X. Xie

Doctor of Philosophy

in

Biomedical Engineering

Stony Brook University

2016

Carbon nanotubes (CNTs) in recent years have been cited to provide great potential for biomedical applications such as drug delivery, imaging and hyperthermia. In particular, it has been shown that they are able to interact with a broad array of electromagnetic radiation, including microwaves. The latter is of great interest for cancer imaging and therapy due to its non-ionizing nature and unique balance of spatial resolution and penetration depth, as well as ability to thermally ablate tumor tissue. Combined with microwaves, CNTs can serve as a platform with high selectivity of microwave absorption, enabling selective microwave thermal therapy, and effective means for synergistically enhancing effect of radiotherapy, chemotherapy and immunotherapy in cancer treatment. However, impurities, poor dispersibility and lack of fine-tuning of intrinsic physicochemical properties hinder CNTs' utility for these applications.

We present a CNT formulation useful for such applications by investigating different purification methods and elucidating the impact of physicochemical changes on the microwave dielectric properties of CNT dispersions. Based on these results, we developed a formulation of CNTs with high dispersibility and microwave dielectric and heating properties by fine-tuning an acid purification method. We also performed *in vivo* acute toxicity and ultrasound and photoacoustic imaging of the CNTs after injecting directly into tumors of mice models to demonstrate safety and validate the ability of the CNTs to be monitored in real-time. This work brings CNTs closer to their potential to serve as microwave hyperthermia agents.

Dedication Page

To my mother for all her love and support.

TABLE OF CONTENTS

LIST OF ABBREVIATIONS

AC: Amorphous carbon

AFM: Atomic force microscopy

AL: Average length

ANOVA: Analysis of variance

ANSI: American National Standards Institute

ATCC: American type culture collection

AUC: Area under curve

BWF: Briet-Wigner-Fano

CNT: Carbon nanotube

CVD: Chemical vapor deposition

DI: Deionized

DMF: Dimethylformamide

DSPE–PEG: 1,2-distearoyl-sn-glycero-3-phosphoethanolamine-N-[carboxy(polyethylene glycol)-5000]

DTT: Dithiothreitol

DWCNT: Double-walled carbon nanotube

EPR: Enhanced permeation and retention

FDA: Food and Drug Administration

FTIR: Fourier transform infrared spectroscopy

H&E: Gill's III Hematoxylin and Eosin

HIFU: High intensity focused ultrasound

HPLC: High-performance liquid chromatography

HSP: Heat-sensitive protein

ID/IG: Ratio of the D- to G-band intensity

ID: Injected dose

MRI: Magnetic resonance imaging

MWCNT: Multi-walled carbon nanotube

NIR: Near infrared

NIST: National Institute of Standards and Technology

PA: Photoacoustic

RBM: Radial breathing mode

RF: Radiofrequency

RPM: Revolutions per minute

RPMI medium: Roswell Park Memorial Institute medium

SAR: Specific absorption rate

SDS: Sodium dodecyl sulfate

SWCNT: Single-walled carbon nanotube

TEM: Transmission electron microscopy

TGA: Thermogravimetric analysis

TUNEL: Terminal deoxynucleotidy transferase biotin-dUTP nick-end labeling

US: Ultrasound

UV: Ultraviolet

UV-vis: Ultraviolet-visible light

SELECT PUBLICATIONS

1. **Shawn X. Xie**, Fuqiang Gao, Sunny C. Patel, John H. Booske, Susan C. Hagness, Balaji Sitharaman, "*Effect of synthesis and acid purification methods on the microwave dielectric properties of single-walled carbon nanotube aqueous dispersions*". Applied Physics Letters. 2013 Sep; 103(13): 133114.

2. **Shawn X. Xie**, Fuqiang Gao, Sunny C. Patel, John H. Booske, Susan C. Hagness, Balaji Sitharaman, "*Clinically Relevant CNT Dispersions with Exceptionally High Dielectric Properties for Microwave Theranostic Applications*". IEEE Transactions on Biomedical Engineering. 2014 May; 61(11): 2718-2723.

3. **Shawn X. Xie***, Tejen Shah*, Chelsea Marks*, Balaji Sitharaman. "*Locally delivered nanoparticle platforms for cancer treatment*". (In preparation) **2016** (*contributed equally)

4. **Shawn X. Xie**, Stephen Lee, Cassandra Suhrland, Kenneth R. Shroyer and Balaji Sitharaman. "*In vivo toxicity assessment and photoacoustic and ultrasound imaging of clinically relevant carbon nanotubes*". (In preparation) **2016**

5. Sayan M. Chowdhury, **Shawn X. Xie**, Justin Fang, Stephen Lee, Balaji Sitharaman. "*Nanoparticle-Facilitated Membrane Depolarization Induced Receptor Activation: Implications on Cellular Uptake and Drug Delivery*". ACS Biomaterials Science & Engineering. (In review) **2016**

6. Fuqiang Gao, **Shawn X. Xie**, Susan C. Hagness, John H. Booske, Balaji Sitharaman, "In Vivo *Microwave Dielectric Spectroscopy of Breast Tumor Xenografts with Intra-Tumoral Injections of SWCNT Dispersions*," Instrumentation and Measurement Technology Conference, 2013 IEEE International, pp. 1441-1444.

7. Fuqiang Gao, **Shawn X. Xie**, John H. Booske, Susan C. Hagness, Balaji Sitharaman, "*Functionalized Carbon Nanotube Theranostic Agents for Microwave Diagnostic Imaging and Thermal Therapy of Tumors*", 2014 European Association on Antennas and Propagation, The Hague, Netherlands.

I. Chapter 1: Background and Specific Aims

A. *Literature Review and Research Question*

1. Cancer treatment

Cancer is a profound disease that can attack virtually any organ in the body and typically manifests in clinical diagnoses as a tumor – an abnormal growth of cells within the body that disrupt normal activity. Physicians typically treat cancer with radiotherapy, remove the tumor from the host surgically, thermally ablate the tumor, induce toxic environments within or raise the body's own defenses against the cancer tissue. Radiation therapy typically results in undesired toxicities and side effects from ionizing radiation, and the issue with surgery is that the removal of the cancerous tissue can lead to recurrence from incomplete removal. The wound healing stimulated by the surgery can also directly benefit any cancer cells left behind and cause rapid regrowth and metastasis. For patients with small, unresectable tumors or who are poor surgical candidates, thermal ablation may be considered; however, issues include incomplete ablation, destruction of healthy tissue, disease recurrence and inferior outcomes.[1] On the other hand, the issue with inducing toxic environments or raising the body's own defenses, i.e. in chemotherapy or immunotherapy, is that these treatments are administered systemically, leading to whole body toxicity and serious side effects. While killing the cancer cells, the drug can cause a loss of quality of life and major ailments associated with the side effects caused by healthy tissue exposure to the therapeutics. These side effects can be avoided if the therapeutics being administered were targeted specifically and delivered to only the cancer tissue. [2]

2. Local delivery

Locally delivered therapeutics can treat cancer in a more efficient and less harmful way than traditional systemic methods. Here, local delivery is defined as any route of administration

that is not intravenous or oral. This form of targeted therapeutic administration allows for greater efficacy, retention, and localization of the particular therapeutic delivered. By bypassing the bloodstream and gastrointestinal system, there is a greater likelihood of the drug reaching the targeted tissue and a decreased likelihood of off-target inefficiencies and systemic toxicity. Local delivery allows for better retention, enhanced uptake, increased temporal and spatial control of drug release, increased ability to bypass biological barriers, and an increased susceptibility to temperature and pH changes. Distinct types of local delivery strategies include but are not limited to the following: 1) intratumoral, 2) intraductal, 3) intravesical, 4) subcutaneous 5) intraperitoneal, 6) inhalation, 7) intra-arterial embolization, and 8) systemic release of nanoparticles followed by local delivery of drugs.

Intratumoral

Intratumoral delivery is a local delivery method that introduces therapeutics into the tumor tissue directly. This is effective in many types of cancer models, such as human glioma models. One reason for this is that intratumoral injections allow one to completely elude the BBB, which is a key barrier to overcome when dealing with brain tumors. This method is also necessary when being combined with techniques or therapeutics that could be especially damaging to healthy surrounding tissue. This includes hyperthermia and thermal ablation to locally ablate cancer cells. This would be highly dangerous if not contained within the tumor tissue only. This is also essential when the therapeutic is cytotoxic. It is important to limit healthy cell exposure to external agents that interact with the body to produce cytotoxic or carcinogenic compounds. Intratumoral delivery of therapeutics can create toxic environments within the tumor to induce cell death while avoiding similar effects on healthy cells.

Intraductal

Intraductal delivery is useful in the treatment of cancers that localize in organs that have vast ductal systems, such as the pancreas. This type of delivery takes advantage of the anatomy of the specific organ into which the therapeutic is to be delivered. It is more effective in the treatment of these cancers than intratumoral because it allows the treatment of multiple tumors within a single organ rather than just a single tumor. The therapeutic can infiltrate a larger portion of the organ where multiple cancer sites might have occurred while retaining minimal exposure of healthy tissue to the potentially harmful effects of the therapeutic.

Intravesical

Intravesical delivery is used primarily in the treatment of bladder cancers. In this method, therapeutics are injected directly into the bladder through a catheter, instead of being injected into a vein or swallowed. Therapeutics delivered this way typically target cancer cells on the bladder lining and do not reach the deeper layers of the bladder wall, the kidneys, ureters or urethra.

Subcutaneous

Subcutaneous delivery is a direct injection into the adipose tissue under the skin. This method of injection is best used when the therapeutic is slightly toxic or has a short half-life. This is due to the fact that adipose tissue is less vascularized compared to organs and thus less therapeutic is needed in order to have an optimized delivery. Furthermore, subcutaneous injection allows for slow diffusion of the therapeutic into systemic circulation, and thus sustained release of therapeutics can be achieved to a certain extent.

Intraperitoneal

Intraperitoneal delivery is an injection in which the therapeutic is released into the body cavity known as the peritoneum, or the central body cavity. Intraperitoneal delivery is an effective method of local delivery for several reasons: it can achieve a higher concentration and longer half-life compared to intravenous delivery, and it can mimic the effects of systemic delivery if needed due to diffusion of drugs out of the peritoneum or into the lymphatic vasculature. Although the concentration and effectiveness of intraperitoneal delivery is greater in-situ, the ability to act systemically can aid in the treatment of lymphatic cancers; however, the efficacy is dependent upon the therapeutics' ability to diffuse into the target tissue. This technique is also useful when the model system or patient suffers from low blood pressure and as a result, intravenous or other types of local deliveries may be challenging and potentially painful. Lastly, intraperitoneal delivery may be favored over other local delivery methods due to its non-invasiveness. For example, an intratumoral injection into a glioma model may present challenges due to the intricate structure of the brain.

Inhalation

Inhalation involves aerosolized forms of a therapeutic that is loaded with a common cancer drug. The premise of inhalation is simple; the aerosolized particles are breathed in and specifically used to target pulmonary cancers. Often times, the therapeutics themselves have natural affinity for lung cells, further bolstering the local nature of this method.

Intra-arterial embolization

Intra-arterial embolization involves the use of therapeutics to clot and close off the vasculature that supplies the cancer cells with nutrients needed to proliferate. This method is

usually combined with a second local delivery method so that a therapeutic will be delivered and the target tissue will be isolated to enhance retention. Although any local delivery method can be used, embolization is commonly paired with intratumoral injections. This approach is best used in the treatment of cancers that affect highly vascularized organs such as the liver, kidney or heart because cells in these organs are accustomed to an ample blood supply. Embolization cuts off that blood supply and thus creates a less favorable environment for tumor growth.

Systemic release and local delivery

Systemic injection, although traditionally a systematic method, can be made effectively local when combined with nanoparticles that are able to detect different environmental conditions and only release therapeutics when these conditions are met. These environmental factors, among others, include pH, temperature, and charge. These factors are usually different between malignant and healthy tissue; thus the drug can be selectively released inside the tumor microenvironment while injected systemically. This method can be very useful for almost any type of cancer because most tumor microenvironments are largely the same. Furthermore, this delivery method can detect and treat remote metastatic cancer sometimes even before these second site tumors are detected by modern imaging techniques.

3. Hyperthermia and thermal ablation

In the context of cancer treatment, thermal therapy is not only applied as an effective method for ablation of tumors, but also as a modulator of the body's immune response. Accumulating evidence indicates that mild-to-moderate hyperthermia (38-42 °C) can increase the immunogenicity of tumor cells and enhance the activities of immune cells, including antigen-presenting cells, T-cells, and natural killer cells,[3,4] acting as a sensitizer for radiation therapy or chemotherapy.[5,6] On the other hand, thermal ablation of tumors involves the local application of

5

extreme temperatures, either high or low, to induce irreversible cell damage and ultimately tumor apoptosis and coagulative necrosis. Hyperthermia with cytotoxic temperatures (>43 °C) or cryoablative temperatures (-20 to -40 °C) can ablate tumor cells directly and release tumor-specific antigens *in situ* for the induction of an antitumor immune response.[4] Thermal ablation has been used to treat many tumor types, including adrenal glands, bone, breast, head, kidney, liver, lung and neck cancers; it is primarily used to treat small, unresectable tumors or for patients who are poor surgical candidates. A particularly novel and burgeoning area of research in ablation focuses on immune-modulation. Prior literature have reported a natural remission of distant untreated metastases after tumor ablation, generating excitement about possible systemic immune responses induced by thermal ablation.[7,8,9] This has piloted a whole new area of research that has broad implications for immunotherapy and combinatorial treatments.

Combining thermal therapy with a conventional treatment such as radiotherapy or chemotherapy can address issues such as incomplete or heterogeneous destruction of tumors. In these strategies, chemotherapy can enhance tumor cell death in the periphery since, at sub-lethal temperatures, these zones may recover from reversible damage. Heat-sensitive proteins (HSPs) that protect against injury can be suppressed by the combination of thermal ablation with nanoparticle-delivered therapies that enhance apoptosis or suppress HSPs. Conceptually, the synergy between radiotherapy and thermal ablation lies in the notion of 'reciprocal zones of efficacy'.[1] Radiotherapy resistance typically occurs at the hypoxic center of the tumor because radiation depends on the presence of oxygen. Hyperthermia is well-known to induce increased vasodilation and vascular permeability, which leads to increased oxygenation and radiotherapy efficacy. Furthermore, immune responses that are induced by thermal ablations alone are usually

too modest to effectively destroy established tumors.[10] Thus strategies involving a combination of thermal ablation and immunostimulant drugs have been implemented in previous studies.[11,12]

In terms of thermal modalities, the most widely used are radiofrequency (RF), microwave and cryo-ablation. Newer technologies, such as high intensity focused ultrasound (HIFU) and laser ablation are less well studied. Table I summarizes the differences among the ablation modalities.[1,13,14]

Table I. Summary of thermal ablation modalities

	RF	Microwave	Laser	Cryo-ablation	HIFU
Frequency	375-500 kHz	900-2450 MHz	560-1064 nm	None	200 KHz-3.5 MHz
Mechanism	Alternating electric field raises temperature and causes coagulation	Alternating electric field raises temperature and causes coagulation	Light energy converted to heat and causes coagulation	Rapid cooling to freeze and damage tissue	Ultrasonic beams raise temperature and causes coagulation
Advantages	Short treatment time (<5 min)	Greater heating profile and less severe heat sink effects than RF, short treatment time (1-2 min), good wave penetration for tissue (2-4 cm)	Linear lesions capable, thermometry with MRI	Larger ablation volumes than RF, less thrombogenic than RF, less procedural pain, can preserve ablated tissue	Thermometry with MRI, precise control of energy delivery
Dis-advantages	Ablation zone includes healthy tissue, power deposition attenuates rapidly from electrode	Ablation zone includes healthy tissue	Size of ablation zone limited by tissue carbonization, scattering and attenuation high	Catheters complicated and expensive, control of freezing and thawing volume	Cost of equipment very high, acoustic windows and coupling required

4. Microwaves

The microwave frequency regime is of great interest for both imaging and hyperthermia due to its non-ionizing nature and unique balance of spatial resolution and penetration depth in

tissue. In tissue, microwaves interact with endogenous polar molecules, such as water, amino acids, peptides, and proteins, which influence the macroscopic dielectric properties – relative permittivity and effective conductivity – of the tissue. Generally speaking, these properties are fundamentally different quantities as the former is a static while the latter is a dynamic property. Relative permittivity is a measure of how much a material transmits or opposes a microwave field, and can be related to refractive index n (used for optics) as

$$n = \sqrt{\varepsilon_r \mu_r},$$

where ε_r is the relative permittivity and μ_r is relative permeability.[15] For non-magnetic materials, μ_r is very close to 1, thus n approximates $\varepsilon_r{}^{1/2}$. Differences in ε_r lead to scattering of microwaves, and thus heterogeneity of ε_r in bulk tissue ultimately lead to differential scattering, which is the basis for microwave imaging based on inverse scattering.[16] Effective conductivity, on the other hand, is property that forms the basis of microwave hyperthermia. In the context of electromagnetic energy absorption, the specific absorption of rate (SAR) of a tissue is given by

$$SAR = \frac{\sigma_e |E|^2}{2\rho},$$

where E is the electric field, σ_e is the effective conductivity, and ρ is the mass density. Furthermore, for the case in which microwave power dissipation in a region is uniform and so rapid that thermal diffusion can be neglected, the temperature rise can be described as

$$\Delta T = \frac{SAR * \tau}{C_p} = \frac{\sigma_e |E|^2 * \tau}{2\rho * C_p} = \frac{|E|^2 * \tau}{2\rho * C_p} * \sigma_e \propto \sigma_e$$

where τ is the microwave pulse length C_p is the specific heat, and SAR is the specific absorption rate.[17] The above equation shows that the amplitude of the temperature change, or heating rate, is proportional to the effective conductivity of the tissue.

The dielectric properties of a tissue or malignant tumor can further be influenced by exogenous agents, such as nanoparticles. Moreover, such agents could enhance the selectivity of microwave absorption to facilitate targeted thermal therapy, and as previously mentioned, can be an effective means for synergistically enhancing the effect of radiotherapy, chemotherapy or immunotherapy in the treatment of cancer.

5. Nanoparticles

Nanoparticles are extremely small molecules that can be defined as have at least one dimension less than a micron. These particles are highly advantageous in treating diseases such as cancer due to their small size, which enables them to more easily extravasate in tissue structures, such as vascular pores. The ability to permeate tissue makes for a therapeutic that can treat the cancer at the source. Nanoparticles are also useful because they can be chemically modified and respond to different types of external energy such as ultrasound, magnetic fields, lasers, and microwaves. In addition, nanoparticles can act as drug carriers as well as the therapeutic themselves. As carriers, they can aid in mediating an interaction between the host cell and the desired therapeutic by releasing the drug inside the tumor cell.

Carbon-based nanoparticles are uniquely composed of chemically modifiable sp^2 carbon atoms bonded together that yield unique electrical, thermal, and spectroscopic properties. These modifiable properties allow them to act as delivery vehicles for drugs, nucleic acids, and imaging agents. They also allow them to act as multifunctional imaging and therapeutic platforms as delivery vehicles for drugs, nucleic acids, contrast and hyperthermia agents. Moreover, carbon nanotubes (CNTs), such as single-walled, double-walled and multi-walled carbon nanotubes (SWCNTs, DWCNTs and MWCNTs, respectively), have enormous potential in cancer therapy due to their unique interactions with electromagnetic radiation over a broad range of

frequencies.[18,19,20,21] In particular, recent microwave-frequency experiments show that aqueous CNT dispersions can significantly enhance the effective dielectric properties of tissue-mimicking materials[22] and breast tumor xenografts [Chapter II]. Furthermore, among the prospective agents investigated for dielectric enhancements, such as copper, gold, microbubbles, carbon buckyballs, and CNTs, only CNTs increased both the permittivity and conductivity of the medium.[23,24,25] Such enhancement may be exploited for microwave-based thermal therapy of tumors. **However, the factors that affect the microwave response of CNTs are poorly understood; moreover, strategies that enable adequate accumulation of CNTs in tumors and ability to characterize the distribution of CNTs *in vivo* have to be implemented.** Thus, the overall objectives of this proposal are 1) to synthesize highly dispersible carbon nanotubes with high microwave dielectric properties and characterize their physicochemical properties, and 2) to investigate their safety and distribution *in vivo*.

B. Specific Aims

Specific Aim 1: To investigate the changes in microwave dielectric and physicochemical properties of CNTs induced by acid treatment. The effect of synthesis method and acid treatment on the microwave-frequency dielectric properties of CNTs will be investigated. The physicochemical properties will be investigated by Atomic Force Microscopy (AFM), UV-Vis spectroscopy, Raman spectroscopy, and Thermogravimetric analysis (TGA).

Specific Aim 2: To formulate an acid treatment that creates water-dispersible CNT formulations with high microwave dielectric properties. An acid treatment method and its conditions will be carefully chosen to synthesize highly dispersible CNT formulations with high microwave dielectric properties. The physicochemical properties will be investigated by Atomic Force Microscopy (AFM), Raman spectroscopy, Thermogravimetric analysis (TGA), Fourier transform infrared spectroscopy (FTIR), and osmolality.

Specific Aim 3: To investigate the acute toxicity of the CNT formulations *in vivo* following intratumoral injection and CNT distribution via histology. The CNT formulations will be evaluated *in vivo* for acute toxic effects in breast cancer xenograft models at a dose that facilitates microwave hyperthermia by body weight measurements and histopathology. The distribution of the CNTs within the tumor will also be evaluated by histology.

Specific Aim 4: To evaluate the distribution of CNTs *in vivo* following intratumoral injection via ultrasound and photoacoustic imaging. The NIR absorption, photoacoustic signal and echogenicity of the CNT formulations will be characterized under ultrasound (US) and photoacoustic (PA) imaging. The intratumoral distribution of CNTs will then be assessed *in vivo* following injections into tumors grown on mice.

II. Chapter 2: Preliminary Dielectric Measurements of Breast Tumor Xenografts *In Vivo* following Intratumoral Injections of Carbon Nanotubes

Preface

Portions of this chapter have been reproduced from

Fuqiang Gao, Shawn X. Xie, Susan C. Hagness, John H. Booske, and Balaji Sitharaman. *In vivo* microwave dielectric spectroscopy of breast tumor xenografts with intra-tumoral injections of SWCNT dispersions. In Instrumentation and Measurement Technology Conference (I2MTC), 2013 IEEE International, pp. 1441-1444. IEEE, 2013.

The authors listed in the above conference paper have contributions towards the data reported in this chapter.

A. Abstract

We present *in vivo* microwave dielectric spectroscopy measurements and histology of human breast tumor xenografts in mice after intratumoral injections of single-walled carbon nanotubes (SWCNTs). Dielectric properties measurements were conducted on 29 mouse tumors in their intrinsic states (pre-injection) and after a variety of intratumoral injections (baseline without SWCNTs, and different concentrations of SWCNTs) using an open-ended coaxial probe technique. Analyses of bright-field and Raman imaging of histological sections were conducted to minimize uncertainty in observed changes in dielectric properties. Comprehensive analysis of both the dielectric properties and histology revealed at least a 10% relative permittivity enhancement effect from the SWCNTs with input solution concentrations ranging between 3 mg/mL and 7 mg/mL.

B. Introduction

The validity of the *in vivo* microwave effect of SWCNTs requires careful investigation to assess their clinical value. In this study, we report preliminary microwave dielectric spectroscopy studies following intratumoral injections of aqueous SWCNTs in breast tumor xenografts grown on nude mice. Analysis of the data was conducted using histology as well as bright-field and Raman imaging.

C. Research Design and Methods

1. Preparation of SWCNT dispersions in PEG

SWCNTs (90 wt%) grown by catalytic chemical vapor deposition were obtained from CheapTubes. 1,2-distearoyl-sn-glycero-3-phosphoethanolamine-N-[carboxy(polyethylene glycol)-5000] (DSPE–PEG) was purchased from NOF America Corporation. DSPE-PEG was dissolved in deionized (DI) water at 0.1 wt% and SWCNTs were dispersed in appropriate

volumes of aqueous DSPE-PEG to obtain the desired SWCNT-DSPE-PEG concentrations. For better dispersion, the SWCNT-DSPE-PEG solutions were bath-sonicated at 100 W for 30 min and then probe-sonicated at 150 W for 3 minutes. All sonication steps were performed within 8 hours before any animal experiment.

2. Cell culture

Human breast cancer cells (MDA-MB-231) were acquired from the American Type Culture Collection and were maintained in RPMI medium from Life Technologies at standard incubation conditions (37°C, 5% CO_2). The cells were supplemented with 10% fetal bovine serum from Thermo Scientific and 1% penicillin-streptomycin from Life Technologies. All cells were cultured for up to 4 days before passaging, in which they were pelleted by centrifugation at 1000 rpm for 5 minutes and resuspended in complete RPMI media.

3. Xenograft model

Immunodeficient female nu/nu mice at 43-56 days old from Charles River Laboratories were subcutaneously injected in the left and right flanks with 10^6 MDA-MB-231 cells. The injections were prepared by combining suspensions of 2-2.5 x 10^6 cells/100 µL cold 1x PBS with 100 µL Matrigel Basement Membrane Matrix from BD Biosciences. Mice were monitored weekly for tumor formation by caliper measurement until tumors reached 0.5-1 cm in diameter (4-6 weeks after injection). All animal studies were approved by the Institutional Animal Care and Use Committee of Stony Brook University.

4. *In vivo* measurements of dielectric properties

Measurements of the dielectric properties were conducted with the mouse positioned on a vertically-adjustable benchtop jack. The skin layer over the tumor was partially removed to allow for direct probe contact with the tumor surface. The tip of a narrow-diameter (4.2 mm at the tip)

14

flange-free coaxial probe[26] with a sensing depth of 2 mm was positioned firmly on the surface of the tumor tissue. The reflection coefficient at the probe aperture was recorded using an Agilent N5221A vector network analyzer, and post-processing techniques described by Popovic et al[26] were used to extract the dielectric properties (relative permittivity and effective conductivity) over the 1-6 GHz frequency range. We conducted reference liquid (DI water, methanol, and 1-butanol) measurements before each tumor measurement to ensure continued accuracy of our method.

Each mouse was placed under isoflurane anesthesia prior to experiments. For each measurement, the probe tip was positioned on the surface of the tumor, and baseline dielectric measurements were conducted for 15 minutes. The mouse was then lowered from the tip of the probe, and 100 µL solutions of DSPE-PEG or SWCNT-DSPE-PEG were injected through a 25 gauge (25G) needle right underneath the tumor surface. A 30 gauge needle was also inserted similarly near the first needle to reduce back pressure in the injection site and provide a conduit for any leakage. The injection was completed within 5 minutes. If there was any leakage of solution from the injection site that would interfere with the contact between the dielectric probe and the tumor (i.e. the solution would directly contact the probe), we stopped the procedure and restarted the experiment on a different tumor. This was done to make sure that the dominant dielectric response of our measurements was from the tumor tissue, and not from surface fluids. Once the needles were removed, the mouse was raised back up into the original position with the probe tip contacting the tumor surface. Dielectric measurements then continued until 30 minutes after the probe was first placed on the tumor. At the end of the measurements, the probe position was marked on the tumor using both green and purple India ink for contrast, and the mice were euthanized to allow for tumor resection and preparation for histology.

We performed two types of control measurements in order to accurately assess the effect of the injected SWCNTs on the dielectric properties of the tumor. The first type is referred to as "Baseline-Needle"; in this sham control experiment, we followed the protocol described above, but injected nothing through the needle. The goal of this control was to identify the needle insertion effect, if any, on the dielectric properties of the tumor. The second type is referred to as "Baseline-DSPE-PEG"; here we again followed the protocol described above, but injected 100 µl of DSPE-PEG solution (instead of SWCNT-DSPE-PEG). The goal of this control was to determine the effect of the DSPE-PEG solution on the dielectric response of tumor. For SWCNT-DSPE-PEG injections, we prepared 3, 5, and 7 mg/mL solutions and injected 100 µL of a given solution in a tumor.

5. Histology

The entire tumor along with the skin covering the tumor site was resected and placed in 10% neutral buffered formalin from Fisher Scientific. Tissues were incubated overnight at 4°C and transferred into 1x PBS before processing by standard formalin fixation, paraffin embedding, and sectioning. 5 µm sections were deparaffinized and rehydrated in a graded series of ethanol solutions, from 100% to 75%. Sections were then stained using Gill's III Hematoxylin and Eosin (H&E) followed by dehydration through a graded series of ethanol solutions from 75% to 100%. Brightfield images of the tissue sections were taken using an Axiovert 200M inverted microscope from Zeiss.

6. Raman imaging

Samples were subjected to dispersive point-by-point Raman spectroscopy using an excitation laser at 532 nm on an Alpha300 R Confocal Raman microscope from WITec through

a 20x objective lens. As an indicator of SWCNTs, the G-band (around 1580 cm^{-1}) intensity was collected, and area maps were constructed and mapped.

7. Bright-field and Raman imaging-based exclusionary criteria

We established exclusionary criteria based on information provided by histology and Raman imaging in order to minimize uncertainty in the observed changes in dielectric properties of the tumors post-injection. There were three reasons for a particular sample to be excluded from the dielectric results presented in this study:

i. The India ink was missing or indiscernible from the histological section, making determination of the probe position impossible,

ii. There was no presence of SWCNTs in a tumor sample in which we injected SWCNTs.

iii. There were SWCNT aggregates on the tumor surface in contact with probe.

D. Results

Recent microwave-frequency experiments have shown that aqueous CNT dispersions can significantly enhance the effective dielectric properties – relative permittivity ε_r and effective conductivity σ_e – of tissue-mimicking materials[22] and breast tumor xenografts.[27] In the latter study, we conducted dielectric measurements of tumors grown on mice after injecting CNT dispersions intratumorally.
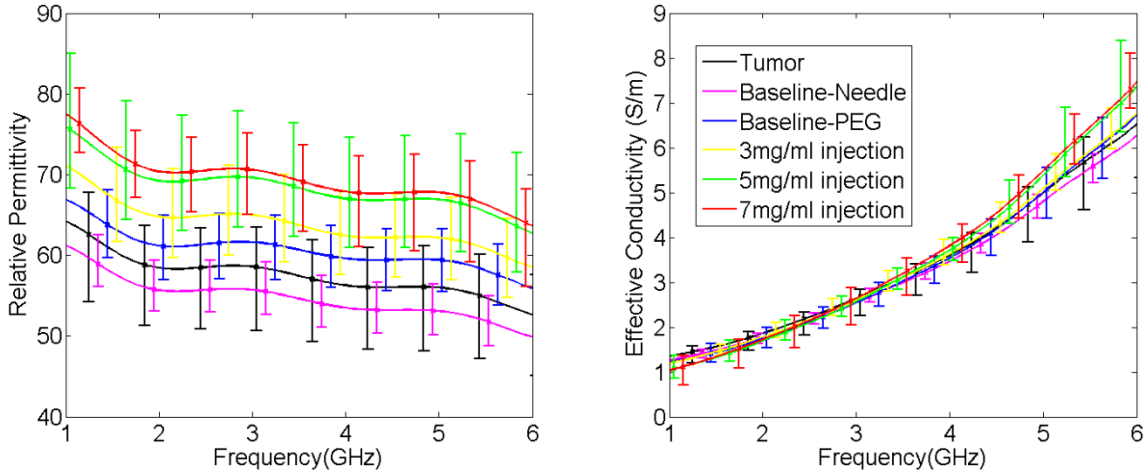
Figure 1. Relative permittivity (left) and effective conductivity (right) of tumor with varying concentrations of SWCNT injections. *Data collected by Fuqiang Gao.*

Figure 1 shows the average dielectric properties for each group with the bars spanning the minimum and maximum values. Each "Tumor" data curve was recorded 10 minutes after the probe was first placed on the tumor and represents the innate dielectric properties of that particular sample. Each "Baseline-Needle" data curve was recorded 30 minutes after the probe was first placed on the tumor, or about 10 minutes after the needles were removed. The relatively large error bars in the intrinsic tumor measurements are mainly due to tissue heterogeneity and subsequently large variations in innate dielectric properties.[28] On the other hand, the variations in the "Baseline-Needle" measurements are likely attributed to minor and random changes in interstitial fluid distribution within the tumor upon needle insertion. The data corresponding to the injection curves were recorded 30 minutes after the probe was first placed on the tumor, or about 10 minutes after completion of the injection.

Table II. Summary of data presented in Figure 1 at 4 GHz

Type of Measurement	Average Permittivity (4 GHz)	Average Conductivity (4 GHz)	Average Percent Change of Permittivity	Average Percent Change of Conductivity	# of Samples (n)
Tumor prior to needle insertion	56.22	3.64 S/m	-	-	34
Baseline-Needle	53.44	3.51 S/m	-4.9%	-3.6%	6
Baseline-PEG	59.57	3.59 S/m	6.0%	-1%	6
3 mg/ml*	62.37	3.67 S/m	6.0%	-2.8%	5
5 mg/ml*	66.97	3.76 S/m	14.2%	-0.3%	6
7 mg/ml*	67.82	3.86 S/m	15.7%	2.4%	6

*Values reported relative to Baseline-Needle

Table II summarizes the dielectric properties of the different post-injection tumors at 4 GHz from Figure 1. From these results, we see that the presence of DSPE-PEG solution alone ("Baseline-DSPE-PEG") slightly elevated (+6.0%) the relative permittivity of the tumor. We also see that, on average, there was at least a 10% relative permittivity enhancement effect from the SWCNTs with concentrations at or above 3 mg/mL relative to Baseline-Needle. The relative enhancements in conductivity (-2.8-2.4%) were smaller, but non-negligible. We did not observe a significant difference in relative permittivity (14.2% and 15.7%, respectively) between the 5 and 7 mg/mL pre-injection solutions. This was presumably due to the fact that the actual concentration of the 7 mg/mL injections was similar to that of the 5 mg/mL, as noted previously. The relatively large variability bars are attributed to the fact that the SWCNT distribution inside the tumor and within the sensing volume of the dielectric probe varies greatly across the tumors (as suggested by histology).

Upon applying the histological exclusionary criteria, we eliminated five cases – one based on criteria (i), zero based on criteria (ii), and four based on criteria (iii) – involving SWCNT-DSPE-PEG injections from further analysis. For each case involving SWCNT-DSPE-

PEG injection that was included, we confirmed the presence of SWCNTs using Raman; there were no cases involving SWCNT-DSPE-PEG injections in which SWCNTs did not show up in at least one histological section. As an example, Figure 2 shows a representative section of a tumor that had a significant increase in dielectric properties following 5 mg/mL SWCNT-DSPE-PEG injection. We subjected this sample to Raman mapping to verify that the cluster of SWCNTs within the red box (Figure 2, *A*) was not extruding beyond the tumor surface that was in contact with the dielectric probe. As shown by the Raman intensity map (Figure 2, *C*) of the highlighted bright-field region (Figure 2, *B*), there is, in fact, a thin layer of tissue between the probe and the cluster of SWCNTs. The presence of SWCNTs in the area map is depicted by the distinctive G-band peak at about 1585 cm^{-1} in the red spectrum (Figure 2, *D*); thus we kept this sample in our data analysis.
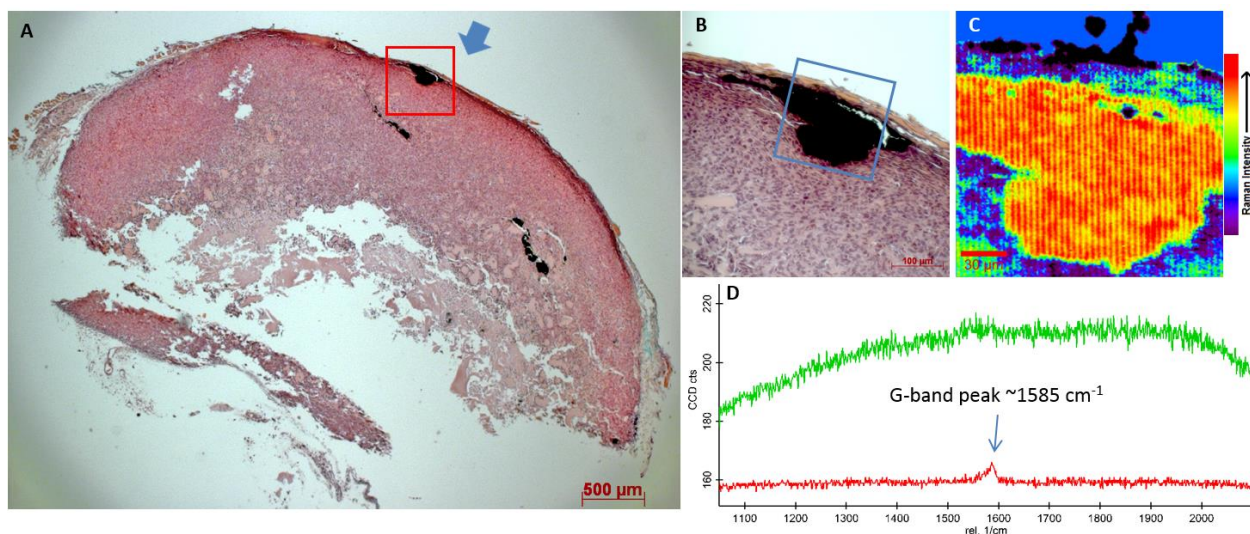
Figure 2. Raman mapping of an included 5 mg/mL SWCNT-DSPE-PEG sample that significantly enhanced the tumor's dielectric properties. (A) Bright field image of histological tumor section at 2.5X. Blue arrow indicates the approximate probe center on the tumor surface during the microwave measurements. (B) Bright field image at 20X of the corresponding region highlighted within the red box in (A). (C) Area map of Raman G-band intensity of region highlighted within blue box in (B). Black regions are areas with no apparent signal (Raman scattering). (D) Representative Raman spectra of area map. Green spectrum is the representative spectrum for green intensity regions. Red spectrum is the representative spectrum for red intensity regions.

20

Figure 3 depicts an example case in which there was an insignificant change in dielectric properties following SWCNT-DSPE-PEG injection, but SWCNTs showed up clearly in the histological sections. The unexpectedly low change in dielectric properties could be due to inadequate amounts of SWCNTs accumulating within the probe's sensing depth. Furthermore, the probe's sensitivity also drops with depth, and thus the distribution of SWCNTs is another important factor in the measurements. We note that due to nonlinear deformations in the tissues after histological processing, we could not establish a histological exclusionary criterion based on SWCNT distribution within the sensing volume of the probe. Thus, we kept this case in our data solely based on confirmed SWCNT presence in a section.
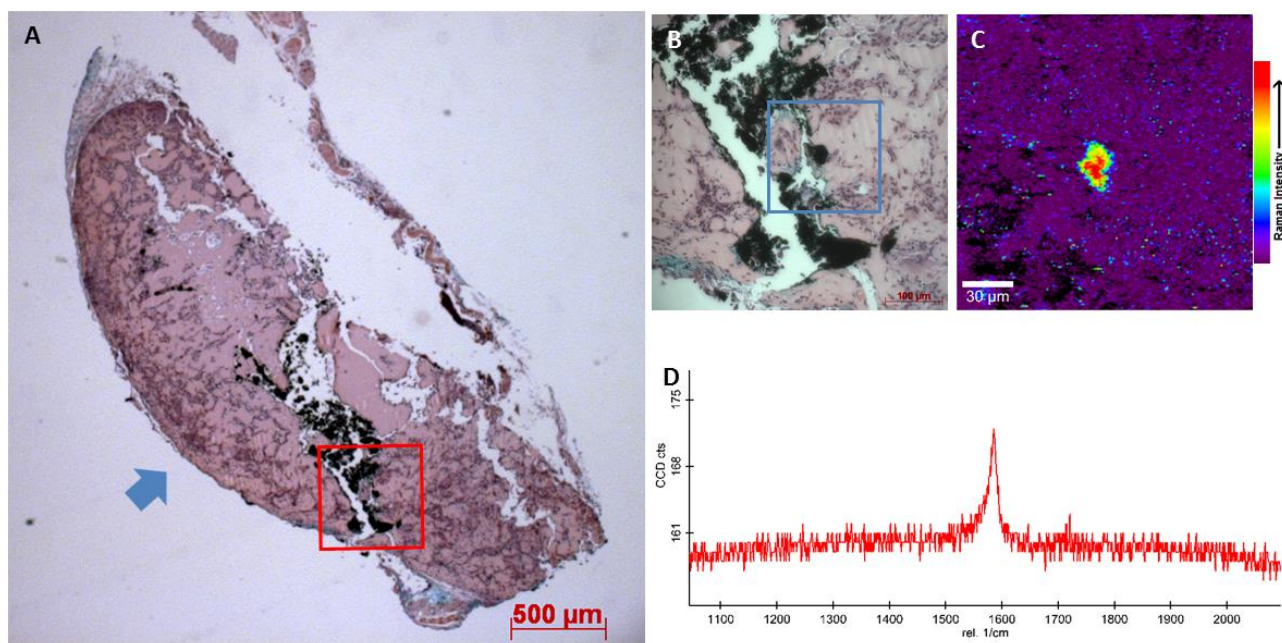
Figure 3. Raman mapping of an included 3 mg/mL SWCNT-DSPE-PEG sample that did not significantly enhance the tumor's dielectric properties. (A) Bright field image of histological tumor section at 2.5X. Blue arrow indicates the approximate probe center on the tumor surface during the microwave measurements. (B) Bright field image of the corresponding region highlighted within the red box in (A). (C) Area map of Raman G-band intensity of region highlighted within blue box of (B). Black regions are areas with no signal (Raman scattering). (D) Representative Raman point spectrum of red region in area map.

E. Discussion

In this study, we characterized the dielectric properties of mouse tumors before and after intratumoral SWCNT injections. To our best knowledge, this is the first study that provides empirical evidence of SWCNTs enhancing the microwave dielectric properties of tissues *in vivo*. As a valuable reference for future comprehensive studies on the *in vivo* microwave effects of nanoparticle theranostic agents, this study provides a preliminary evaluation of the efficacy of SWCNT-based agents. We note that we achieved relatively modest enhancements in the microwave dielectric properties (+20% in relative permittivity and +6% in effective conductivity) of tumors following injections of SWCNT-DSPE-PEG at concentrations that were at and beyond the SWCNT dispersion limits in water through non-covalent methods (evident from the needle-clogging observations). We expect that increasing solubility could lead to significantly higher enhancements via both increased concentration and dispersion homogeneity, which can potentially be achieved through covalent functionalization methods. Ultimately, maximizing the concentration delivered to tumor sites while minimizing offsite delivery is perhaps the quintessential challenge in cancer nanomedicine. For cancer diagnostics and therapy, the most common approaches to this challenge have been to exploit both passive and active targeting via the enhanced permeation and retention effect in tumors and ligand-receptor interactions.[29] The latter has seen development for SWCNTs since their size and unique physiochemical properties bestow them the ability to append many targeting ligands along the length of their carbon sheaths. [30-34] In previous reports, SWCNTs have been functionalized to both tumor-targeting monoclonal antibodies and small peptides for enhanced tumor accumulation;[35,36] however, whether active targeting was used or not, the amount of accumulation has been low relative to the injected dose (ranging between 0.2-15 % ID/g) when

injected systemically. It is well documented that the main properties influencing the distribution and targeting of nanoparticles in the body include size, shape, coating, as well as ligands and charge.[37] Moreover, some of these very factors, such as nanotube length and degree of covalent functionalization, can and have been shown to affect the microwave dielectric properties of SWCNT dispersions.[38] We also note that the dielectric properties reflect macroscopic properties of host mediums, and thus depend on how stably dispersed the SWCNTs are, which in turn could be affected by many other factors, such as the presence of surfactants, pH, and ionic strength. All of these factors should be systematically investigated in the development of SWCNTs for *in vivo* microwave-frequency applications alongside the continued growth of nanoparticle delivery strategies. Indeed, as suggested by our studies, the adequate accumulation of SWCNTs in tumors for enhancement in microwave dielectric properties may benefit greatly from the use of local delivery methods, such as image-guided intra-arterial or intratumoral delivery, which can dramatically enhance nanoparticle uptake in tumors.[39] Similar delivery strategies may be considered alongside the optimization of carbon nanotube formulations for the latter's development as clinical therapeutic platforms for microwave-frequency treatment of cancer.

III. Chapter 3: Investigating Physicochemical Properties of Carbon Nanotubes that Affect Their Microwave-Frequency Dielectric Properties

Preface

Portions of this chapter have been reproduced from

Shawn X. Xie, Fuqiang Gao, Sunny C. Patel, John H. Booske, Susan C. Hagness, and Balaji Sitharaman. Effect of synthesis and acid purification methods on the microwave dielectric properties of single-walled carbon nanotube aqueous dispersions. Applied Physics Letters 103, no. 13 (2013): 133114.

The authors listed in the above manuscript have contributions towards the data reported in this chapter.

A. Abstract

We characterized the microwave-frequency (0.5-6 GHz) dielectric properties of aqueous dispersions of pristine and purified single-walled carbon nanotubes (SWCNTs). SWCNTs were synthesized by two CVD-based methods and purified using two acid-based purification methods. We characterized the structural and chemical differences across SWCNT samples using Raman analysis, UV-Vis spectroscopy, atomic force microscopy, and thermogravimetric analysis. We found that the dielectric properties of the pristine SWCNT dispersions did not vary with synthesis method, but the dielectric properties of purified SWCNT dispersions were variably impacted by acid purification due to different degrees of morphological and chemical changes in the SWCNTs.

B. Introduction

Pristine SWCNTs contain varying amounts of semiconducting and metallic nanotubes depending on the synthesis method. Oxidative purification, routinely employed to remove impurities such as amorphous carbon and metal catalysts,[40,41,42] alters the SWCNT chemical structure. A large body of work now documents the variability and changes in optical and electronic properties of SWCNT aqueous dispersions due to synthesis method and post-synthesis purification steps.[43] However, no such studies have been reported on potential changes in microwave properties.

In this study, we present a systematic investigation of the effect of SWCNT synthesis and acid purification methods on the microwave dielectric properties of SWCNT aqueous dispersions. The findings of this study underscore the need for and enable the development of quality control strategies to prepare SWCNT-based formulations with consistent properties – a prerequisite for their use in biomedical applications.

25

C. Research Design and Methods

1. Selection and Treatment of CNTs

We used two types of SWCNTs, referred to as Co-SWCNTs and Fe-SWCNTs. The Co-SWCNTs were synthesized by catalytic chemical vapor deposition (CCVD) over cobalt catalysts. The Fe-SWCNTs were synthesized by the high pressure carbon monoxide method with iron catalysts.[44] It is well documented that SWCNT samples synthesized using either of these methods consist of amorphous carbons, semiconducting and metallic SWCNTs, other structured carbon materials (e.g., double walled carbon nanotubes (DWCNT) and/or fullerenes), and metallic catalyst particles.[45] We chose two methods of purification in our study: $HCl+H_2O_2$ and HNO_3 reflux.[46,47] In the $HCl+H_2O_2$ method, 40 mg of SWCNTs were mixed directly with 20 mL of 30% H_2O_2 and 20 mL of 1 N HCl and magnetically stirred at 400 rpm. The mixture was heated and maintained at 60±5 °C for 4 h. At the end of each hour, 20 mL of HCl and 20 mL of H_2O_2 were added to the mixture. On the last cycle, one extra hour was added to allow the H_2O_2 to completely decompose. In the HNO_3 method, each g of SWCNTs was refluxed at 120±5 °C and magnetically stirred at 400 rpm in 150 mL of 3M HNO_3 for 12 h. For both methods, the mixture was cooled to room temperature, diluted with deionized (DI) water, and pelleted by centrifugation at 3000 rpm for 30 min. After discarding the supernatant, the pellet was re-suspended in DI water and filtered through a 0.1 μm pore-sized filter. The product on the filter was then washed thoroughly with DI water until the pH of the washes reached 7.0. The filtered product was then collected by vacuum oven-drying for 12 h at 60 °C.

2. Characterization of the CNTs

    a. Microwave-frequency dielectric properties

Samples for microwave-frequency dielectric measurements were prepared by dispersing the SWCNTs in 0.1 wt% aqueous PL–PEG_{5400}–NH_2 (NOF Corp.), or DSPE-PEG, at 3 mg/mL and sonicating the dispersion in an ultrasonic bath (Fisher Scientific) at 100 W for 12 h. The temperature of the bath was maintained at ~20-40 °C. Three types of test samples were prepared both for Co-SWCNTs and Fe-SWCNTs: one pristine (non-purified), and two purified (one using $HCl+H_2O_2$ and the other using HNO_3); thus a total of six test samples were prepared. We also prepared one control sample from DSPE-PEG only (no SWCNTs). We characterized the dielectric properties of the dispersions over the 0.5-6 GHz frequency range using a flange-free 2.2-mm-diameter dielectric probe (Agilent 85070E-030) and a vector network analyzer (Agilent N5221A). For each sample, we conducted the measurement three times with the probe tip at different depths within the sample.

b. Raman spectroscopy

SWCNTs were dispersed in dimethylformamide (DMF) via bath sonication and dropcasted onto silicon wafers for Raman analysis. Raman spectra of all samples were obtained using a ProRaman-L system (Enwave Optronics) using a 532 nm laser.

c. UV-Vis spectroscopy

SWCNTs were dispersed in DMF at ~10 µg/mL via bath sonication, and the supernatant was collected by centrifugation at 5000 rpm for 15 min. UV-Vis absorption of the supernatant in the 400-1100 nm range was acquired using an Evo300 UV-Vis spectrophotometer (Thermo Scientific) equipped with a xenon lamp as the excitation source.

d. Atomic force microscopy (AFM)

SWCNTs were dispersed in DMF at ~10 µg/mL via bath sonication, and the supernatant was collected by centrifugation at 5000 rpm for 15 min. The AFM samples were prepared by

dropping 10 µL of the supernatant on a polished silicon wafer, followed by drying in a fume hood. Atomic force micrographs using an EasyScan 2 FlexAFM (Nanosurf) operating in the tapping mode were obtained to analyze the lengths and diameters of the SWCNTs. To determine the size distributions, the length and height of at least 70 objects per group from multiple spots on the substrates were measured from the micrographs. Since the deposition of the SWCNTs on the substrate may be kinetically controlled, all AFM samples were prepared from dispersions of about the same concentration and for the same duration of drying; therefore, the relative diameter and length distributions are considered reliable.

e. Thermogravimetric analyses (TGA)

TGA was performed using a thermogravimetric/differential thermal analyzer (Perkin Elmer) in the range of 20-800 °C in air at a scan rate of 5 °C/min.

D. Results

1. Microwave-frequency dielectric properties
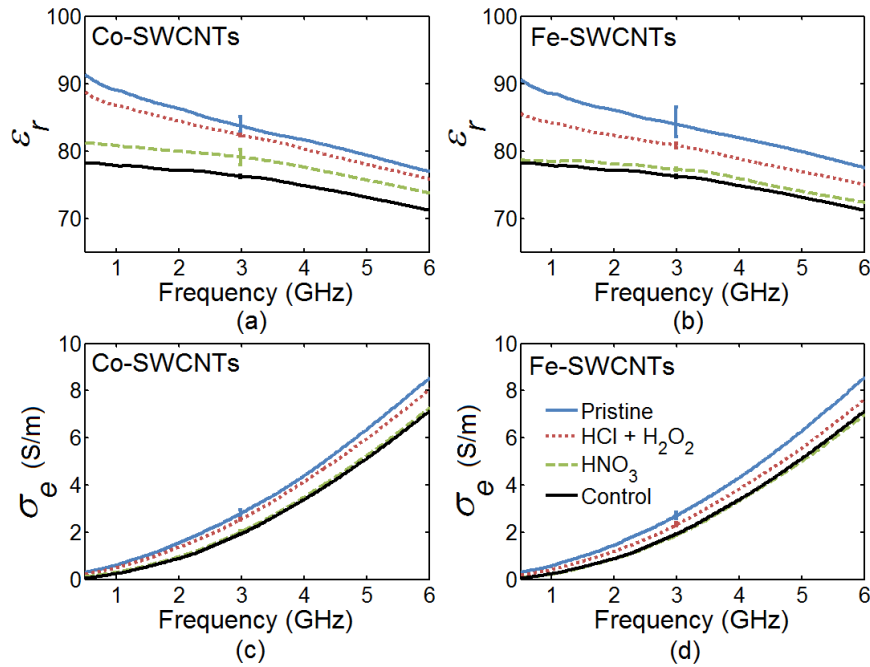
Figure 4: Measured microwave-frequency dielectric properties of aqueous dispersions of pristine and purified (a) Co-SWCNTs and (b) Fe-SWCNTs. *Data collected by Fuqiang Gao.*

Figure 4 shows the measured ε_r and σ_e of the pristine and purified SWCNT dispersions, as well as the control (SWCNT-free solution).[38] Each curve represents the average of three measurements. The bars span the minimum and maximum values of the three measurements to show the variability across measurements for a given sample. Only the variability at 3 GHz is shown; the measured data at other frequencies exhibit similar variability. Figures 4(a) and 4(c) show ε_r and σ_e, respectively, for the three Co-SWCNT dispersions compared to the control. There is a large properties enhancement for the pristine Co-SWCNT dispersion compared to the control. For example, at 3 GHz, the average ε_r increases by 10% and the average σ_e increases by 45%. The dielectric properties of the (HCl+H$_2$O$_2$)-purified Co-SWCNT dispersion are slightly lower than those of the pristine dispersion; for example, at 3 GHz, the average ε_r decreases by 1.6% and the average σ_e decreases by 8.7%. The dielectric properties of the HNO$_3$-purified Co-SWCNT dispersion are closer to those of the control sample than the pristine dispersion. These results show that the HNO$_3$ purification method more severely reduces the microwave-frequency dielectric properties enhancement effect of Co-SWCNTs in dispersion than the HCl+H$_2$O$_2$ purification method. Figures 4(b) and 4(d) display ε_r and σ_e, respectively, for the three Fe-SWCNT dispersions compared to the control. We observe similar trends here. Namely, the pristine Fe-SWCNT dispersion exhibits greatly elevated dielectric properties compared to the control; at 3 GHz, the average ε_r increases by 10% and the average σ_e increases by 40%. Also, both purification methods reduce the degree of enhancement, with HNO$_3$ purification decreasing the enhancement so severely that there is little difference between the HNO$_3$-purified Fe-SWCNT dispersion and the control. By comparing the results for Co-SWCNT and Fe-SWCNT dispersions [Figs. 4(a) with 4(b) and Figs. 4(c) with 4(d)], we conclude the following: (1) both

Co-SWCNTs and Fe-SWCNTs in their pristine state enhance the dielectric properties of the control solution significantly (by at least 10% in ε_r and 40% in σ_e at 3 GHz); (2) in general, acid purification decreases the dielectric properties enhancement effect of both types of SWCNTs; (3) HNO$_3$ purification decreases the enhancement more than HCl+H$_2$O$_2$ purification for both types of SWCNTs; and (4) the decrease in the enhancement due to acid purification is more severe for the Fe-SWCNTs than for the Co-SWCNTs. These results and conclusions suggest that acid purification imposes structural change on SWCNTs and these changes depend on both the type of SWCNTs and the purification method used.

2. CNT size distributions
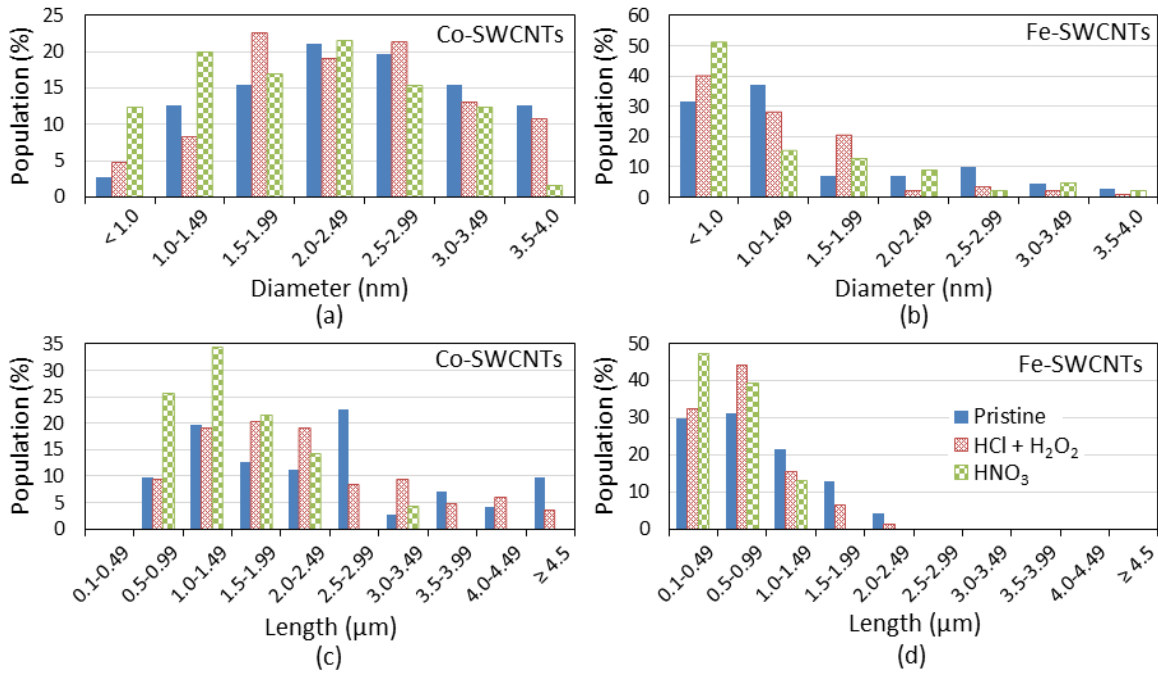
Figure 5: Pristine and purified SWCNT dimensions characterized by AFM. (a) Diameter distribution of the Co-SWCNTs. (b) Diameter distribution of the Fe-SWCNTs. (c) Length distribution of the Co-SWCNTs. Average lengths: pristine = 2.53 µm, purified (HCl+H$_2$O$_2$) = 2.26 µm, purified (HNO$_3$) = 1.45 µm. (d) Length distribution of the Fe-SWCNTs. Average lengths: pristine = 0.74 µm, purified (HCl+H$_2$O$_2$) = 0.64 µm, purified (HNO$_3$) = 0.58 µm.

Figure 5 displays histograms of the distributions of SWCNT diameters and lengths obtained by AFM measurements.[38] The diameter distributions [Figs. 5(a) and 5(b)] reveal a much larger fraction of nanotubes and bundles that are >2 nm due to the presence of double-walled carbon nanotubes (DWCNTs) in the Co-SWCNT samples.[48,49] For both Co-SWCNTs and Fe-SWCNTs, the fractions of small-diameter SWCNTs increased with HCl+H_2O_2 or HNO_3 treatment. Figures 5(c) and 5(d) indicate that, after HCl+H_2O_2 treatment, the average lengths (AL) of Co-SWCNTs and Fe-SWCNTs decreased by ~10.7% and ~13.5%, respectively. These results also indicate that, after HNO_3 treatment, the AL of Co-SWCNTs and Fe-SWCNTs decreased by ~42.7% and ~21.6%, respectively.

3. Raman spectra
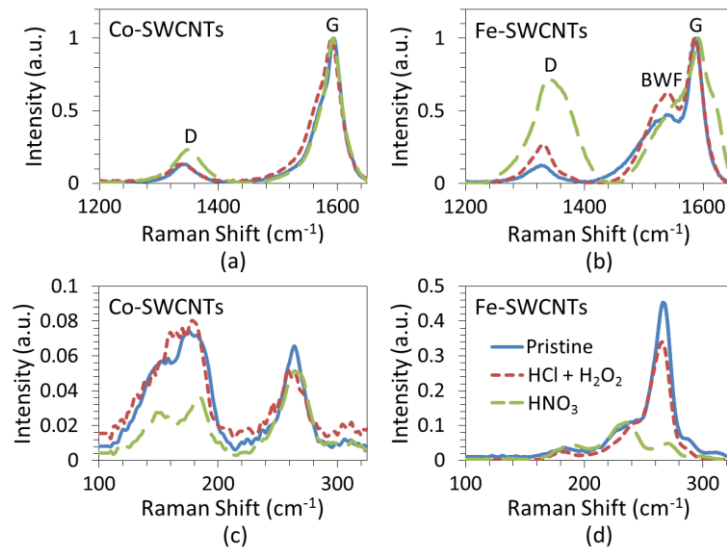
Figure 6: Raman spectra of pristine and purified SWCNTs. (a) D- and G-bands of the Co-SWCNTs. (b) D- and G-bands of the Fe-SWCNTs. (c) RBM mode of the Co-SWCNTs. (d) RBM mode of the Fe-SWCNTs. All spectra were normalized with respect to the G-band intensity.

Figure 6 displays the Raman spectra of the SWCNTs. Figures 6(a) and 6(b) show the relative G (~1590 cm^{-1})- and D (~1340 cm^{-1})-band intensities.[38] The ratio of the D- to G-band intensity (I_D/I_G) is widely used as a measure of the disordered sites on the SWCNT sidewalls, and as an indicator of the oxidation level in the SWCNTs.[50,51] Comparing the pristine and purified Co-

SWCNTs in Figure 6(a), we observed a mild increase in the I_D/I_G ratio after HNO_3 treatment. Fe-SWCNTs showed a mild increase in the I_D/I_G ratio after $HCl+H_2O_2$ treatment and a large increase in the I_D/I_G ratio after HNO_3 treatment. It is well known that the HNO_3-based purification of Fe-SWCNTs could lead to digestion of smaller diameter SWCNTs;[52,53] this digestion produces carbonaceous impurities and disordered carbon that can form a uniform coating around intact SWCNTs.[54,55] Thus the destruction and subsequent coating of SWCNTs could explain the significantly high I_D/I_G ratio of Fe-SWCNTs observed in Figure 6(b) after HNO_3 reflux. The Raman spectra of the Fe-SWCNTs [Fig. 6(b)] also shows a shoulder peak in the G-band ($\sim$1540 cm^{-1}), known as the Briet-Wigner-Fano (BWF) lineshape, attributed to metallic SWCNTs.[56] The intensity of the BWF peak significantly decreases after HNO_3 treatment, which signifies a loss of metallic SWCNTs. Figures 6(c) and 6(d) show the variations of radial breathing mode (RBM) frequencies for Co-SWCNTs and Fe-SWCNTs, respectively. Figure 6(c) shows two distinct peaks below and above 250 cm^{-1}, which indicate the presence of DWCNTs in the Co-SWCNTs.[57] Conversely, Figure 6(d) shows only one distinct peak above 250 cm^{-1}, which indicates the presence of mainly SWCNTs in the Fe-SWCNTs. The relative intensity changes in the RBM frequencies for the purified Fe-SWCNTs and the HNO_3-purified Co-SWCNTs signify a chemical alteration of the nanotubes.[50,51]

4. UV-Vis spectra
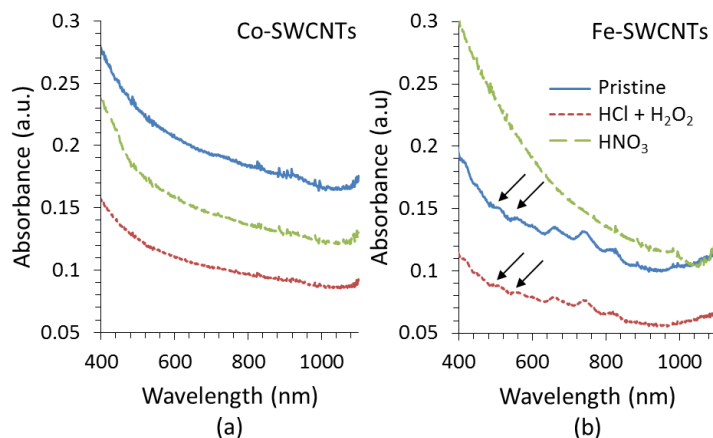
Figure 7: UV-Vis spectra of pristine and purified (a) Co-SWCNTs and (b) Fe-SWCNTs. Arrows highlight metallic bands.

Figure 7 shows representative UV-Vis absorption spectra of the SWCNTs.[38] Figure 7(a) shows that there were no distinct peaks that indicate the Van Hove transitions of pristine or purified Co-SWCNTs. A previous report has attributed this absence of distinct Van Hove peaks within the 400-1100 nm range to a presence of DWCNTs in Co-SWCNT samples.[49] Pristine Fe-SWCNTs show Van Hove transition bands for both metallic (510 and 560 nm) and semiconducting SWCNTs (650, 740, and 820 nm). These bands were largely conserved after HCl+H_2O_2 purification. Conversely, HNO_3 purification completely diminished these bands, implying significant changes in the chemical and electronic structure of Fe-SWCNTs.

5. Thermogravimetric analyses
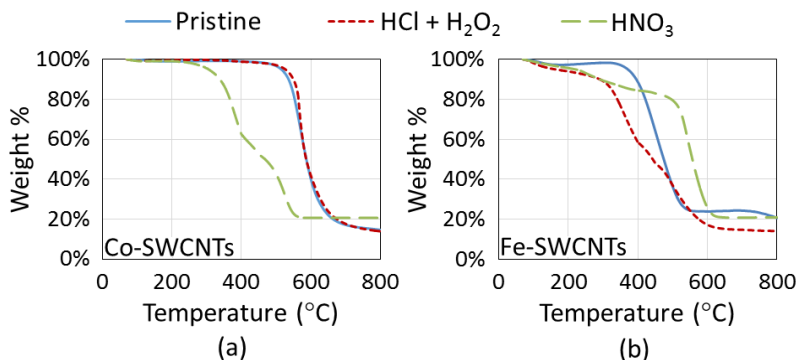
Figure 8: TGA curves of pristine and purified (a) Co-SWCNTs and (b) Fe-SWCNTs. *Data collected by Sunny C. Patel.*

Figure 8 shows the TGA analyses of the SWCNTs.[38] Typically for pristine SWCNTs, the thermal decomposition of amorphous carbon (AC) and SWCNTs is indicated by two weight loss inflections centered at ~350 °C and ~425 °C, respectively; the leftover mass at 800 °C is attributed to residual metal catalyst.[47,58] Figure 8(a) shows that the thermal stability for pristine Co-SWCNTs is actually centered at ~570 °C. This shift from 425 °C to 570 °C can be attributed to the presence of both SWCNTs and DWCNTs in the Co-SWCNT sample, as the thermal stability of pristine DWCNTs is centered at ~630 °C.[59] The TGA curve of the Co-SWCNTs does not change noticeably after HCl+H_2O_2 purification, but is significantly different after HNO_3 purification. Specifically, HNO_3 reflux led to an increase from ~1% to ~40% AC in the sample. The fact that the thermal stability decreased to ~500 °C suggests chemical alteration to the nanotubes. Figure 8(b) shows an increase in AC from ~2% to ~41% and a decrease in the metal catalyst fraction from about 20% to 13% in HCl+H_2O_2-treated Fe-SWCNTs as compared to pristine Fe-SWCNTs. The thermal stability of HCl+H_2O_2-treated Fe-SWCNTs also increased to ~500 °C. A previous report attributes this increase to the partial removal of the metal catalysts that lower the activation energy of SWCNT oxidation.[60] After HNO_3 reflux, the AC content in Fe-SWCNTs increased from ~2% to ~15%. Additionally, the thermal stability of the HNO_3-

treated Fe-SWCNTs increased to ~550 °C compared to their pristine counterparts (~425 °C), and again indicates metal catalyst removal. However, the fact that the relative metal catalyst fraction did not change significantly compared to pristine Fe-SWCNTs indicates a simultaneous decrease in the carbon content after HNO_3 reflux.

E. Discussion

Table III provides a quantitative summary of the results from Figures 4-6 and 8; the values indicate the percent changes in several attributes after purification (by $HCl+H_2O_2$ or HNO_3). It is apparent that the more negative impact of HNO_3 purification on the microwave-properties enhancement effect of both types of SWCNTs (indicated by the larger negative percent change in ε_r and σ_e) is associated with its stronger length-shortening effect (indicated by the larger percent change in AL) and stronger oxidizing effect (indicated by the larger percent change in I_D/I_G), compared to $HCl+H_2O_2$ purification. Although the relative increase in AC for HNO_3-purified Fe-SWCNTs is not as high as that of $HCl+H_2O_2$-purified Fe-SWCNTs, there is a larger AL decrease and I_D/I_G increase, along with a loss of metallic nanotubes [Fig. 7(b)], which collectively result in a larger reduction in ε_r and σ_e. Table III also provides insights into why Fe-SWCNTs exhibit greater reductions in ε_r and σ_e after acid purification compared to Co-SWCNTs.[38] After $HCl+H_2O_2$ purification, the changes in AL, I_D/I_G, and AC of Fe-SWCNTs were all more prominent; after HNO_3 purification, a much larger increase in I_D/I_G and loss of metallic nanotubes [Fig. 7(b)] in Fe-SWCNTs was observed.

TABLE III. Percent change in attributes of purified SWCNT dispersions relative to the pristine SWCNT dispersions.

	Co-SWCNT		Fe-SWCNT	
	$HCl+H_2O_2$	HNO_3	$HCl+H_2O_2$	HNO_3
$\varepsilon_r{}^a$	-2	-6	-4	-8
$\sigma_e{}^a$	-9	-28	-14	-31
AL	-11	-43	-14	-22
I_D/I_G	+1	+75	+113	+475
AC	+0	+39	+39	+13

[a]Value at 3 GHz

In summary, our study demonstrates the following: (1) Aqueous dispersions of pristine Co-SWCNTs and Fe-SWCNTs synthesized by two distinct CVD-based methods, with significant differences in morphology, show similarly elevated microwave dielectric properties compared to a control; (2) Acid-purification-based changes in SWCNT structure and composition – namely, decreases in length and fraction of metallic nanotubes, as well as increases in amorphous carbon and covalent functionalization of SWCNTs depending on the purification method – marginally or dramatically reduce the microwave dielectric properties of SWCNT aqueous dispersions. These findings have important implications in the development of SWCNT-based formulations of microwave-frequency theranostic agents for biomedical applications.

IV. Chapter 4: Synthesizing Highly Dispersible CNT Formulations with High Microwave Dielectric Properties.

Preface

Portions of this chapter have been reproduced from

Shawn X. Xie., Fuqiang Gao, Sunny C. Patel, John H. Booske, Susan C. Hagness, and Balaji Sitharaman. Clinically Relevant CNT Dispersions with Exceptionally High Dielectric Properties for Microwave Theranostic Applications. IEEE Transactions on Biomedical Engineering. 2014; PP: 1.

The authors listed in the above manuscript have contributions towards the data reported in this chapter.

A. Abstract

We present a formulation for achieving stable high-concentration (up to 20 mg/ml) aqueous dispersions of carbon nanotubes (CNTs) with exceptionally high microwave-frequency (0.5-6 GHz) dielectric properties. The formulation involves functionalizing CVD-synthesized CNTs via sonication in nitric and sulfuric acid. The overall chemical integrity of the CNTs is largely preserved, as demonstrated by physical and chemical characterizations, despite significant shortening and functionalization with oxygen-containing groups. This is attributed to the protected inner walls of double-walled CNTs (DWCNTs) in the samples. The resulting CNT dispersions show greatly enhanced dielectric properties compared to a CNT-free control. For example, at 3 GHz, the average relative permittivity and effective conductivity across several 20 mg/ml CNT samples were increased by ~70% and ~400%, respectively, compared to the control. These CNT dispersions exhibit the stability and extraordinary microwave properties desired in theranostic agents for microwave diagnostic imaging and/or thermal therapy.

B. Introduction

The appropriate *in vivo* dose of CNT therapeutic agents has not yet been established for microwave-based thermal therapy. For other *in vivo* therapeutic technologies investigated using small-animal models, the potential CNT dose ranges from units to tens of mg/kg of body weight.[18,61] For example, in a rat model with a blood volume of ~10 ml and a weight of ~0.2 kg, a dose of ~10 mg/kg requires a CNT stock dispersion concentration of ~2 mg/ml, assuming that the maximum injection volume is ~1 ml (i.e. no more than 10% of the blood volume). Higher doses may prove to greatly enhance the efficacy of tumor detection or therapy at microwave frequencies. Furthermore, preclinical pharmacology guidelines established by the U.S. Food and Drug Administration (FDA) suggest assessing safety at doses that are at least 10 times higher

38

than the projected therapeutic dose.[62] Thus future *in vivo* preclinical safety and efficacy studies of CNT therapeutic agents for microwave technologies will require stable CNT stock dispersions that pass through injection needles without clogging at concentrations on the order of tens of mg/ml.

Natural or synthetic amphiphilic macromolecules that are biocompatible are widely employed as dispersing agents in the preparation of aqueous CNT dispersions.[63,64] However, these functionalization strategies only allow stable dispersions of individual or debundled CNTs up to hundreds of µg/ml. Methods employing mixtures of strong acids that covalently functionalize CNT sidewalls with carboxyl or hydroxyl functional groups have been shown to yield stable dispersions of debundled CNTs at concentrations on the order of 10 mg/ml.[65,66] However, this increased CNT dispersibility has generally been accompanied by changes in CNT chemical and physical properties[43,38] that lead to changes in their intrinsic electromagnetic properties. In particular, both decreased length and increased oxidation of CNTs have been shown to reduce the microwave dielectric properties of CNT dispersions.[38] The degree of chemical and morphological change induced by acid-based oxidation methods is highly sensitive to the treatment conditions, such as temperature, time, and whether sonication was employed.[67] We have also recently shown that the dispersible concentration of non-isolated CNTs that can pass through small needles is limited to a few mg/ml.[27]

In this study, we present a method for producing CNT dispersions that satisfy previously unmet criteria for systemically administered CNT-based microwave theranostic agents. Namely, the dispersions of highly debundled CNTs are achieved at high concentrations (i.e. tens of mg/ml) and yet do not clog injection needles; furthermore, they exhibit extremely high dielectric properties at microwave frequencies. Both the stability and microwave properties of these high-

concentration dispersions represent dramatic improvements over what has been achieved previously.[22,27,38] Additionally, we report physical and chemical characterizations that reveal why this particular processing method results in CNT dispersions with such desirable properties.

C. Research Design and Methods

1. Synthesis of highly dispersible CNTs

CNTs synthesized by catalytic chemical vapor deposition over cobalt catalysts were obtained from a commercial vendor (Cheaptubes). The CNTs comprised a mixture of single- and double-walled CNTs. The CNTs were treated as follows. For each treatment batch, 60 mg of CNTs were thoroughly mixed in 60 ml of 3:1 H_2SO_4:HNO_3 with a glass rod. The mixture was bath-sonicated at 100 W for 4 h. The temperature of the bath water was initially 25 ℃. Sonication raised the water temperature to 50 ℃ after two hours, at which point the temperature was maintained at 50 ± 5 °C until completion. The mixture was then cooled to room temperature, diluted with deionized (DI) water at a 1:4 ratio, and pelleted by centrifugation at 4000 rpm for 15 min at 10 ℃. The supernatant acid mixture was discarded and the CNT pellets were collected and resuspended in 50 ml of DI water. The centrifugation, discarding, and resuspension steps were repeated until the supernatant color remained dark, typically between pH 1.0 – 2.0. The mixture was then neutralized with NaOH and filtered through a 0.1 μm pore-sized filter. The product on the filter was washed thoroughly with excess DI water ($\geq$2 ml per mg CNT) and collected in 15 ml of DI water. The suspensions were then aliquoted, and after flash-freezing the aliquots in liquid N_2, the dry product was collected by lyophilization for 24 h. The yield per batch was typically between 80-90%.

2. Characterization of the CNTs

    a. Microwave-frequency dielectric properties

Test samples for microwave-frequency dielectric characterization were prepared by dispersing treated CNTs in DI water with mannitol (Sigma-Aldrich M8429), a sugar excipient used in pharmaceutical formulations for intravenous injections, at CNT concentrations of either 10 mg/ml or 20 mg/ml. It was not possible to create test samples of well-dispersed pristine (untreated) CNTs in water at these high concentrations for measurement comparisons. The concentration of mannitol in DI water was chosen to be 50 mg/ml to achieve an osmolality within the range of blood (290-320 mOsm/kg); the osmolality was confirmed by a single-sample osmometer (Advanced Instruments 3D3). No surfactant or sonication was required in the preparation of the samples. Control samples containing only DI water with mannitol (i.e. no CNTs) were also prepared. All samples were confirmed to be at neutral pH (6.8-7.2) by a benchtop pH meter (Fisher Scientific accumet AB15+ Basic). This ensured that any observed differences in the microwave measurements of the test and control samples were due to the presence of CNTs rather than pH-based effects. We characterized the dielectric properties of the dispersions over the 0.5-6 GHz frequency range using a flange-free 2.2-mm-diameter dielectric probe (Agilent 85070E-030) and a vector network analyzer (Agilent N5221A). We also measured CNT dispersions in vials before and after passing the dispersions through a 25 gauge needle. The heating response of each dispersion was characterized using an experimental setup described previously.[22] We poured the dispersion, after passing through the needle, into a 1.1-mm-diameter glass capillary tube. The tube was then inserted into an S-band rectangular waveguide through a small hole drilled into the center of one of the broad walls of the waveguide. A microwave synthesizer (Agilent, 83623B) and amplifier (Mini-Circuits, ZHL-42W) generated 1 W of continuous microwave power at 3 GHz, which was delivered to the sample via the waveguide. The waveguide was terminated with a matched load to ensure single-

pass microwave illumination of the sample. We used a fluoroptic thermometer (Luxtron 3100) to measure the temperature of the sample over time for 3 min of microwave heating.

b. Raman spectroscopy

Refer to III.C.2.b

c. Fourier transform infrared spectroscopy (FTIR)

Fourier transform infrared (FTIR) spectroscopy was performed on dry powders on a Nicolet 6700 FT-IR spectrophotometer (Thermo Scientific) with a liquid-N_2-cooled DLaTGS detector.

d. Atomic force microscopy (AFM)

Refer to III.C.2.d

e. Thermogravimetric analysis (TGA)

Refer to III.C.2.e

D. Results

1. Microwave-frequency dielectric properties
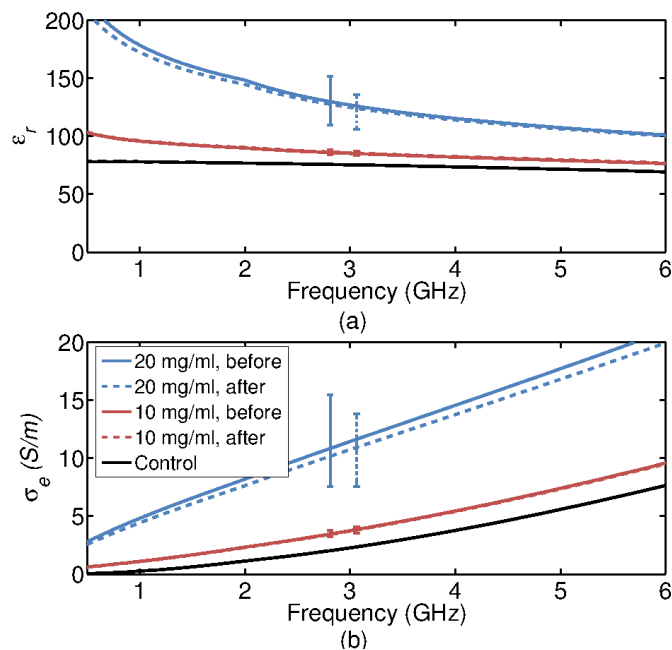
Figure 9: Measured microwave-frequency dielectric properties of aqueous dispersions of treated CNTs, before (solid colored) and after (dashed colored) passing through a 25G needle, compared to the control. Each curve represents the average across three measurements each of multiple samples. *Data collected by Fuqiang Gao*.

Figure 9 shows the measured dielectric properties of several samples for each of the two test sample types (10 and 20 mg/ml concentrations), before and after passing through the 25G needle, in comparison to the control (CNT-free mannitol solution).[68] Each 20 mg/ml curve (blue) represents the average across 12 measurements (four samples, three measurements each). Each 10 mg/ml curve (red) represents the average across 15 measurements (five samples, three measurements each). The vertical bars span the maximum and minimum values; we refer to this spread in the data as the variability in the measured properties. The bars are staggered around 3 GHz to avoid overlap; the bars at 2.9 GHz show the variability before passing through the needle, while the bars at 3.1 GHz show the variability after passing through the needle. The dielectric properties of the CNT dispersions shown in Fig. 9 are significantly higher than those of

the control samples. For example, at 3 GHz, the average ε_r across all dispersions of a fixed CNT concentration, before passing the needle (i.e. the solid colored curves of Fig. 9(a)), is increased by 14% at 10 mg/ml and 68% at 20 mg/ml relative to the control; the average σ_e is increased by 66% and 404% for the 10 and 20 mg/ml samples, respectively. The variability in the 20 mg/ml samples is much greater than the variability in the 10 mg/ml samples. Figure 9 shows that the difference in the dielectric properties of the CNT dispersions before and after passing through the 25G needle is negligible. This is in stark contrast to the behavior of dispersions of non-isolated CNTs, for which the dielectric properties of a sample have been shown to decrease dramatically after passing through a 25G needle due to clogging, even at much lower concentrations than those considered here (i.e. <10 mg/ml).[27] The results of Fig. 9 indicate that the CNTs treated with the method reported here are very well dispersed at these high concentrations. The well-dispersed nature is further confirmed by dielectric-properties stability measurements over time. The dielectric properties of one representative 20 mg/ml sample, monitored over a period of two months, exhibited a variation smaller than the variability observed in Fig. 9.

2. Heating curve
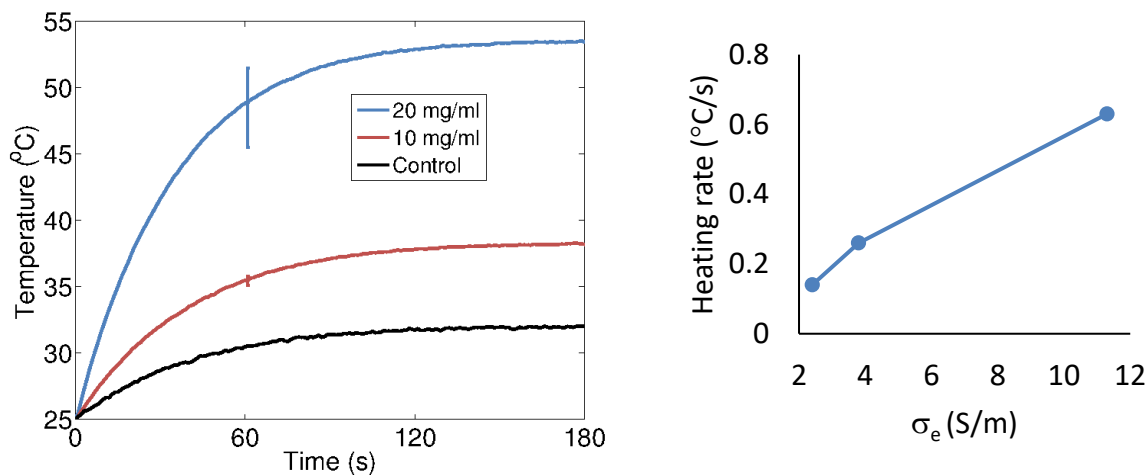
Figure 10: (*Left*) Measured heating response (1 W, 3 GHz) of aqueous dispersions of treated CNTs after passing through the 25G needle, compared to the control. Each curve represents the average across multiple samples of the same concentration. (*Right*) Heating rate vs. σ_e. *Data collected by Fuqiang Gao*.

The greatly enhanced effective conductivity of the samples with CNTs, compared to the CNT-free control, leads to more efficient microwave heating of those samples, as illustrated in Fig. 10.[68] Each curve represents the average temperature of multiple samples at a fixed concentration (four samples for 20 mg/ml, and five samples for 10 mg/ml). The bars span the minimum and maximum temperatures across samples after heating for one minute. The heating rate and the steady state temperature are greatly increased for samples with CNTs. For example, the average heating rate during the first 20 seconds is 0.14°C/s for the control, 0.26°C/s for the 10 mg/ml samples, and 0.63°C/s for the 20 mg/ml samples. When we plot heating rate vs. σ_e, we observed a nonlinear relationship between the two quantities. Since heating rate is related to σ_e by the following relationship [Chapter 1] – $\Delta T = \frac{|E|^2 * \tau}{2\rho * C_p} * \sigma_e$ – we attribute this non-linear effect to both an increase in mass density ρ and specific heat C_p of the dispersions due to increasing concentrations of CNTs.

3. CNT size distributions
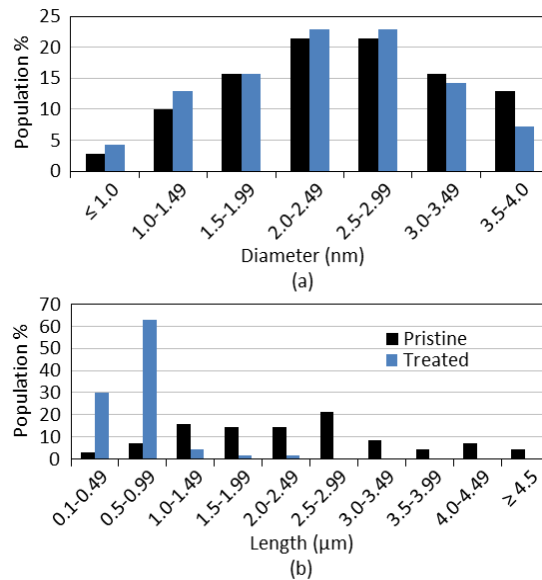
Figure 11: Functionalized CNT dimensions characterized by AFM. (a) Diameter distribution. (b) Length distribution. Average lengths: pristine = 2.43 µm, treated = 0.68 µm.

Figure 11 displays histograms of the CNT diameter and length distributions obtained by AFM measurements.[68] The diameter distribution [Fig. 11(a)] reveals a large fraction of nanotubes and bundles that are >2 nm due to the presence of double-walled carbon nanotubes (DWCNTs) in the CNT samples.[69,70] Figure 11 indicates that, after the acid sonication treatment, the average length (AL) of the CNTs decreased significantly by 72% from 2.43 µm to 0.68 µm, indicating a greater length-shortening effect than previous methods employing either HCl+H_2O_2 or HNO_3 reflux,[38] as summarized in Table IV.

4. Raman spectra
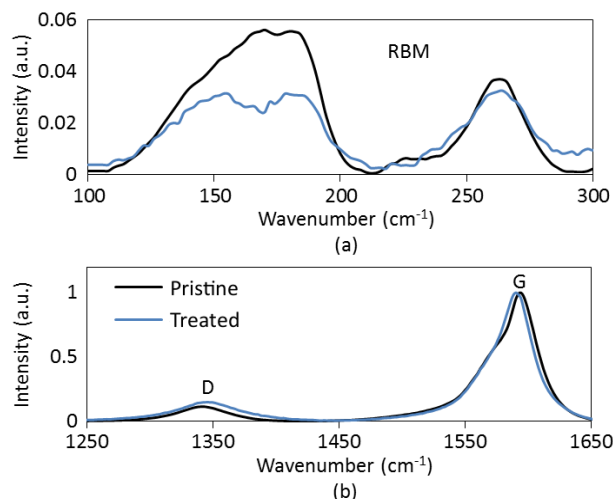
Figure 12: Raman spectra of pristine and treated CNTs. (a) RBM mode. (b) D- and G-bands. All spectra were normalized with respect to the G-band intensity.

Figure 12 displays the Raman spectra of the CNTs.[68] There are two distinct peaks below and above 210 cm^{-1} in the radial breathing mode (RBM) frequencies [Fig. 12(a)], which indicate the presence of DWCNTs.[57] The decrease in the intensity of the lower frequency RBM post-treatment signifies a chemical alteration to the outer diameter of the DWCNTs.[71] Figure 12(b) shows the relative G (~1590 cm^{-1})- and D (~1340 cm^{-1})-band intensities. As a measure of disordered sites and indicator of oxidation level in CNTs,[50,51] the ratio of the D- to G-band intensity (I_D/I_G) increases only mildly from 0.12 to 0.15 (a 25% increase) post-treatment. This

relatively small increase in I_D/I_G may be attributed to the fact that the inner tubes within the DWCNTs are largely protected from chemical alteration. Indeed, larger diameter CNTs are generally less prone to destruction by acids and sonication.[72]

5. FTIR spectra
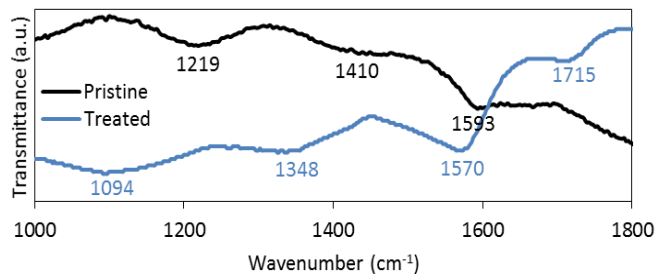
Figure 13: FTIR spectra of pristine and treated CNTs.

Evidence of CNT functionalization is present in the FTIR transmittance spectra of the CNTs, as shown in Fig. 13.[68] The pristine CNT band around 1593 cm^{-1}, which is assigned to the C=C stretching mode,[73] is shifted to a lower frequency around 1570 cm^{-1} after treatment, which may suggest a chemical change in the CNT structure. Indeed, the appearance of new bands around 1348 cm^{-1} and 1715 cm^{-1} in treated CNTs is assigned to the asymmetric SO_2-stretching mode of sulfonic acid (-SO_2–OH) groups and C=O stretching in carboxylic acid (-CO–OH) groups, respectively.[66,74] Furthermore, bands between 1000-1300 cm^{-1} are typically associated with C–O stretching and O–H bending modes of alcoholic, phenolic, and carboxylic groups; specifically, the higher frequency band (~1219 cm^{-1}) present in the pristine CNTs is assigned to phenolic O–H groups, whereas the lower frequency band (~1094 cm^{-1}) present in the treated CNTs is assigned to carboxylic O–H groups.[75] Finally, in the pristine CNTs, there exists a weak band around 1410 cm^{-1}, which is most likely due to sorbed water (O–H in-plane deformation).[76]

6. TGA
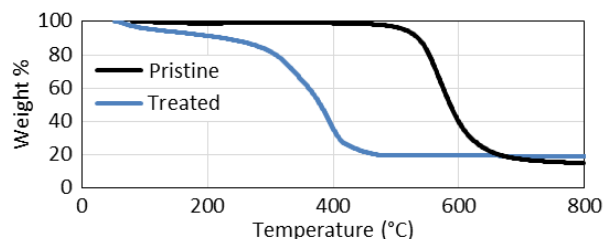
Figure 14: TGA curves of pristine and treated CNTs. *Data collected by Sunny C. Patel.*

The TGA analysis shown in Fig. 14 also confirms the chemical alteration of CNTs and the presence of functional groups, thereby corroborating the Raman and FTIR results.[68] Typically for CNTs, thermal decomposition between 150-350 °C is attributed to loss of functional groups such as -CO–OH groups present on the CNT walls, and decomposition at ~425 °C is attributed to the thermolysis of SWCNTs; the leftover mass at 800 °C is attributed to residual metal catalyst.[47,58,65] It is apparent that the thermal stability for the pristine CNTs is actually centered at ~570 °C, which indicates the presence of both SWCNTs and DWCNTs in the sample, as the thermal stability of pristine DWCNTs is centered at ~630 °C.[59] The TGA traces show that the acid sonication led to increased mass fraction of functional groups from ~1% to ~30% that are present on SWCNT sidewalls and the outer layer of DWCNTs; the thermal decomposition between 350-480 °C can be attributed to leftover and inner layer SWCNTs in the sample.

E. Discussion

In this study, we demonstrate that high-concentration dispersions of CNTs functionalized via a H_2SO_4:HNO_3 treatment with sonication exhibit dramatically enhanced dielectric properties. Chemical and physical characterizations of these functionalized CNTs highlight the properties that yield these high-concentration formulations, as summarized in Table IV.[68]

TABLE IV. Percent change in attributes of treated CNT
dispersions relative to pristine CNT dispersions

	HCl +H_2O_2	HNO_3	H_2SO_4:HNO_3
AL	-11[*]	-43[*]	-72
I_D/I_G	+1[*]	+75[*]	+25

[*]Values from Xie et al.[38]

Although there is a significant reduction in length of the CNTs following the treatment, the overall chemical integrity of the CNTs was largely preserved. The acid treatment employed in this study had a greater length-shortening and chemical preservation effect than alternate acid-reflux methods.[38] The shortened CNT lengths (<1 µm on average) will likely facilitate their use for biomedical applications due to both increased biocompatibility[77] and dispersion stability[78]. Specifically, the shortened length (680 nm average) of the CNTs make them potentially able to extravasate and reach tumor regions when introduced intravascularly since the vascular pores of tumors can be up to 780 nm.[79] Successful functionalization by the addition of carboxylic and sulfonic acid groups on the outer CNT sidewalls is largely responsible for the stable and high CNT concentrations (≥10 mg/ml) reported in this study. Empirical evidence thus far and theoretical principles of strong microwave field enhancement by large-aspect-ratio conductors suggest that the use of DWCNTs for microwave medical applications may be preferred over SWCNTs. This is because DWCNTs offer both an exterior layer that can be functionalized for water solubility and an interior layer that can mitigate changes to the CNT's intrinsic electromagnetic properties by chemical treatments. In summary, the CNT formulations reported in this paper show high potential as microwave-frequency theranostic agents.

V. Chapter 5: Investigating the Acute Toxicity of the CNT Formulations *In Vivo* Following Intratumoral Injection and CNT Distribution via Histology

Preface

Shawn X. Xie., Stephen Lee, Cassandra Suhrland, Kenneth R. Shroyer and Balaji Sitharaman. *In vivo* toxicity assessment and photoacoustic and ultrasound imaging of clinically relevant carbon nanotubes. *Manuscript to be submitted for publication*.

The authors listed in the above manuscript have contributions towards the data reported in this chapter. The authors also thank Ms. Sonya Lorrain of the Research Histology Core Lab of Stony Brook University for technical assistance.

A. Abstract

In this study, we describe the use of highly dispersible carbon nanotubes (CNTs) with high microwave dielectric properties as a proof-of-concept CNT platform that is safe when injected *in vivo* and can be imaged under both ultrasound and photoacoustic imaging *in vivo*. In this part of the study, we did not report any toxicity 1 day and 14 days after CNT injections by body weight and organ histology. Our results support the enormous potential of CNTs as microwave thermal therapy agents that can be delivered safely and imaged in real-time.

B. Introduction

Carbon nanotubes (CNTs) represent a potentially powerful tool in cancer therapy and imaging. In particular, CNTs have also been shown to be promising heating agents for microwave-based thermal therapy of cancer due to their strong interaction with microwaves and ability to enhance the dielectric properties of tissue.[80] This ability is influenced by CNT morphology and chemistry, which ultimately affect CNT biocompatibility and dispersibility.[38] Stable dispersions of CNTs at high concentrations (>10 mg/ml) have been possible via methods employing covalent functionalization. However, this increased CNT dispersibility has generally been accompanied by changes in CNT chemical and physical properties that lead to changes in their intrinsic electromagnetic properties. In particular, both decreased length and increased oxidation of CNTs have been shown to reduce the microwave dielectric properties of CNT dispersions.[38] Thus, we created a novel formulation of highly dispersible CNTs that exhibit extremely high dielectric properties at microwave frequencies.[81] Prior to translating these CNTs into a clinically relevant setting, their potential toxicity *in vivo* should be examined. In light of this, the present work was designed to evaluate acute toxic effects of the CNTs when locally injected into a tumor.

C. Research Design and Methods

1. Preparation of CNT Dispersions

Previously synthesized CNTs were dispersed at 20 mg/ml in DI water with mannitol. The concentration of mannitol in DI water was ~50 mg/ml to achieve an osmolality within the range of blood (290-320 mOsm/kg); the osmolality was confirmed by a single-sample osmometer (Advanced Instruments 3D3). Control samples was prepared with DI water and mannitol only. All samples were sterilized via UV treatment for 30 min prior to *in vivo* studies.

2. Cell Culture

Human breast cancer cells (MCF7) were acquired from the American Type Culture Collection (ATCC) and maintained in RPMI medium from Life Technologies at standard incubation conditions (37°C, 5% CO_2). The cells were supplemented with 10% fetal bovine serum from Thermo Scientific and 1% penicillin-streptomycin from Life Technologies. All cells were cultured for up to 4 days before passaging, in which they will be pelleted by centrifugation at 1000 rpm for 5 minutes and resuspended in complete medium.

3. Xenograft Model

Immunodeficient male nu/nu mice (n = 6 per group) at 43-56 days old from Charles River Laboratories were subcutaneously injected in the right flanks with 10^6 MCF7 cells/100 µL under manual restraint. The injections were prepared by combining suspensions of 10^6 cells/50 µL cold 1x PBS with 50 µL Matrigel Basement Membrane Matrix from Corning. Mice were monitored weekly for tumor formation by caliper measurement until tumors reached ~300 mm^3 (3-4 weeks after injection). The tumor volumes were approximated according to the formula for an ellipsoid:[82,83]

$$\text{volume} = \frac{\pi * \text{length} * \text{width} * \text{depth}}{6}$$

All measurements were performed in triplicate. Animal studies were approved by the Institutional Animal Care and Use Committee of Stony Brook University.

4. Acute Toxicity

Each mouse was placed under isoflurane (1-5% in O_2) anesthesia prior to injections. Intratumoral injections were adjusted accordingly to be 10% tumor volume (~30 µL). Acute toxicity was assessed in all major organs (heart, lungs, liver, kidneys, spleen, intestines) after 1 day and 14 days via histology. Body weight was assessed every two days. The animal groups are summarized in Table V.

Table V. Study design for *in vivo* acute toxicity

Group	Dose*	# Animals	
		Day 1	*Day 14*
Sham Control	-	6	6
Vehicle Control	10% tumor volume	6	6
CNTs + Vehicle	10% tumor volume; 2 mg/cm^3 in tumor	6	6

5. Histology

The resected tumors and organs were placed in 10% neutral buffered formalin from Fisher Scientific. Tissues were incubated overnight at 4°C and transferred into 1x PBS before processing by standard formalin fixation, paraffin embedding, and sectioning. 5 µm sections were deparaffinized and rehydrated in a graded series of ethanol solutions, from 100% to 75%. Sections were then be stained using Gill's III Hematoxylin and Eosin (H&E) followed by dehydration through a graded series of ethanol solutions from 75% to 100%. Brightfield images

of the tissue sections were taken using an Axiovert 200M inverted microscope from Zeiss. Slides were dictated by the Research Histology Core Laboratory at Stony Brook University Hospital.

6. Statistics

Statistical analyses between tumor volumes were performed using a two-sample t-Test, and for all comparisons, the minimal level of significance was set at $p < 0.05$.

D. Results

1. Body Weight and Tumor Volume

Following intra-tumoral injections of CNTs, sham and vehicle controls, we monitored the body weights and tumor volumes of the mice every 2 days for 14 days – Figure 15 shows the respective averages along with corresponding max and min values. During our experiments, we did not notice any obvious sign of toxic side effect for CNT-injected mice within the 14 days; neither death nor significant body weight drop was noted across the treatment groups. Furthermore, we did not observe any significant tumor suppression following the injection of the CNTs compared to sham control ($p = 0.18$ at Day 14).
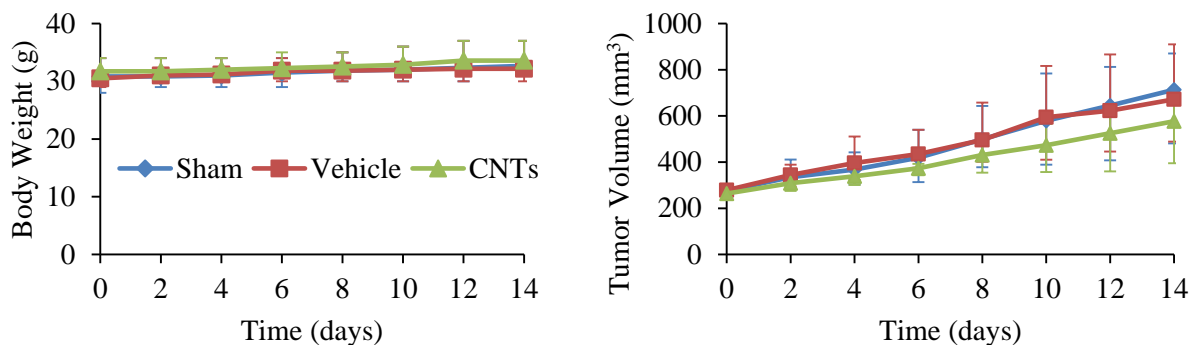
Figure 15: (Left) Body weight over time. (Right) Tumor volume over time. Error bars denote min and max values ($n = 6$).

2. Acute Toxicity and Histology

After the *in vivo* study was completed, we performed histology on major organs and tumors of the mice. In agreement with the results from body weight measurements, histopathology results also indicate no obvious damage or lesions to any major organs at Day 1 or 14, as seen in Figure 16. In characteristic sections of the tumors, the controls and CNT samples show heterogeneous but similar (~50:50) distribution of necrotic (pink) and viable (purple) regions; we note that the degree of necrosis seen in different sections of the same tumor ranged between ~25-75%, and this variation was observed across all groups (Figure 17A-C). The degree of necrosis in the tumors is most likely due to the tumor outgrowing the available supply of nutrients while grafted on the mice, which is typical of these tumor models due to a low degree of vascularization. We observed that the CNTs displaced the extracellular matrix in the sections and were sequestered in pocket regions, with no indication of cellular uptake at Day 1 (Figure 17D). By Day 14, we observed that tumor cell growth led to cellular infiltration into the pocket regions of CNTs, resulting in more dispersed areas of CNTs trapped within extracellular matrices or necrotic regions within the entirety of the tumor (Figure 17C&E). We also observed the presence of red blood cells in areas of vascularization and within coincidental pockets of sequestered CNTs (Figure 17D&E), while the presence of lymphocytes, neutrophils, and plasma cells outside the tumor surfaces indicates mild acute inflammation towards the tumor, which is unrelated to the presence of CNTs (Figure 17F).
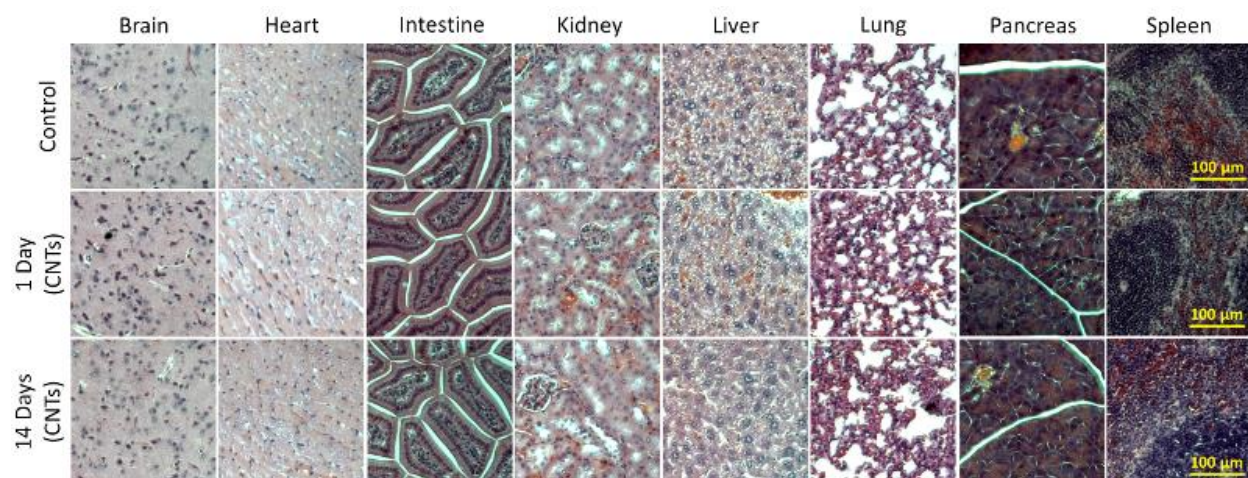
Figure 16: Representative H&E stained images of major organs including brain, heart, intestine, kidney, liver, lung, pancreas and spleen collected from control (Sham at Day 1) untreated mice and CNT-injected mice at 1-day and 14-days post-injection. Dose of CNTs was 2 mg/cm^3 in the tumor. No obvious organ damage or lesion was observed for CNT-treated mice. Scale bar represents 100 µm.
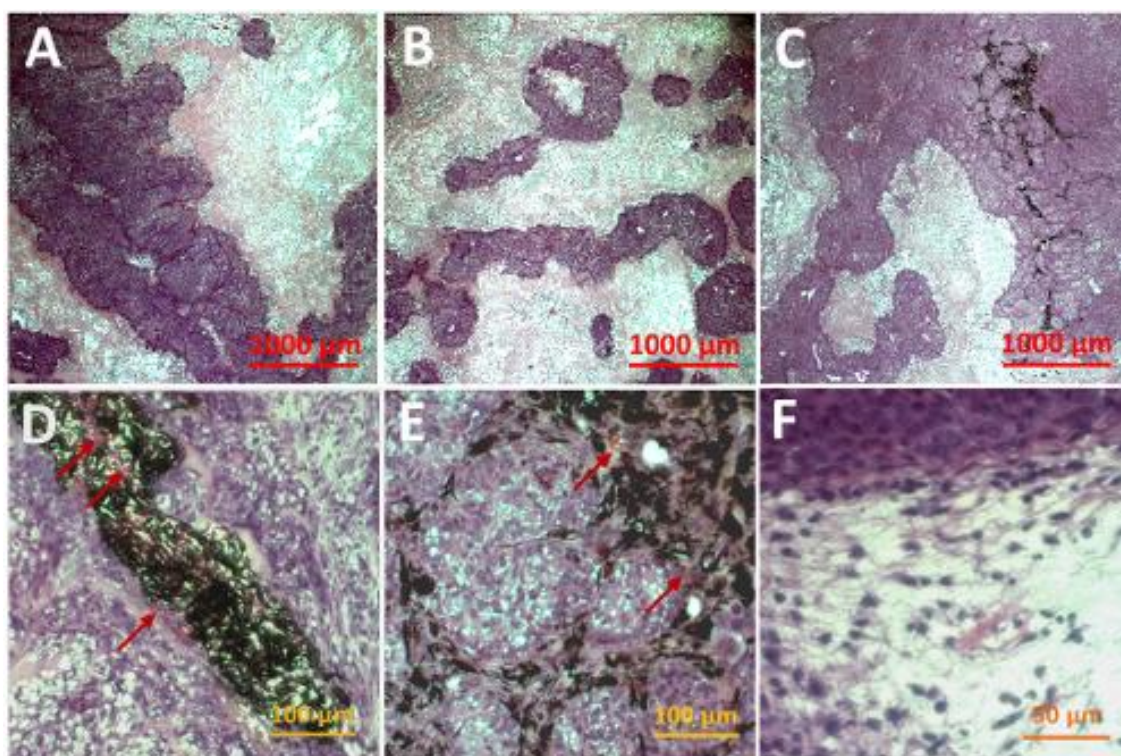
Figure 17: Representative H&E stained images of tumors. (A-C) Day 14 images of sham control, vehicle control and CNT injections, respectively. Black regions highlight presence of CNTs. Red scale bars represent 1000 µm. (D, E) Day 1 and 14, respectively, images of CNT-injected tumors. Red arrows denote red blood cells. Yellow scale bars represent 100 µm. (F) Image of lymphocytes, neutrophils and plasma cells outside the surface of a tumor, indicating mild inflammation towards tumor tissue. Orange scale bar represents 50 µm.

56

E. Discussion

In this study, we demonstrate that the CNT formulation in this study does not induce any obvious acute toxicity signs (based on body weight and histology of major organs) when injected directly into subcutaneous tumors in mice. Although we did not expect to see a therapeutic effect by the CNTs, we note that tumor volume measurements (Figure 15) suggest a trend towards minor inhibition of tumor growth following injection of the CNTs. Based on histology, this trend may be attributed to physical inhibition of tumor cell growth in regions where the CNTs are sequestered and displaced or trapped in extracellular matrix (Figure 17). Although it has been suggested that CNTs may adsorb micronutrients, it is unlikely this is a factor since functionalization and imparting hydrophilicity has been shown to suppress adsorption;[84] we also did not observe any histological correlation between the presence of CNTs and necrosis in the tumor tissue. We attribute the sustained presence of CNTs in the tumor tissue after 14 days post-injection to the physical environment of the subcutaneous tumor model – low degree of vascularization and high physical inhibition by cancer cell infiltration – forcing the injected CNTs to be sequestered in pockets of extracellular matrix or necrotic tissue, which ultimately leads to low clearance of CNTs over time. Given tumor models with higher degrees of vascularization, the clearance of the CNTs over time may increase significantly, especially if injections were directed nearby to blood vessels under image guidance. Overall, there was no histological correlation between the presence of CNTs and inflammatory cells or degree of tumor necrosis. We also did not observe any obvious toxicity to the major organs following injection of CNTs based on histology. These results support the use of direct tumoral injections as a method to locally and safely deliver CNTs into target tumor sites.

VI. Chapter 6: To Evaluate the Distribution of CNTs *In Vivo* Following Intratumoral Injection via Ultrasound and Photoacoustic Imaging

Preface

Shawn X. Xie., Stephen Lee, Cassandra Suhrland, Kenneth R. Shroyer and Balaji Sitharaman. *In vivo* toxicity assessment and photoacoustic and ultrasound imaging of clinically relevant carbon nanotubes. *Manuscript to be submitted for publication*.

The authors listed in the above manuscript have contributions towards the data reported in this chapter. The authors also thank Mr. Andrew Heinmiller and Ms. Carly Warren at VisualSonics, Inc. for their technical assistance.

A. *Abstract*

In this study, we describe the use of highly dispersible carbon nanotubes (CNTs) with high microwave dielectric properties as a proof-of-concept CNT platform that is safe when injected *in vivo* and can be imaged under both ultrasound and photoacoustic imaging *in vivo*. In this part of the study, we assessed the near-infrared spectroscopic and echogenic properties of the CNTs. We demonstrated an ultrasound signal 6x as intense as a water-based control for the highest concentration of CNT dispersions, which translated to high echogenic signals *in vivo*; the average photoacoustic signal of the highest concentration of CNT dispersions was 3x that of diluted methylene blue, and we also observed an average change in photoacoustic signal greater than 4x throughout the tumor post-injection of CNTs. Our results support the enormous potential of CNTs as microwave thermal therapy agents that can be delivered under US image guidance and quantified non-invasively via PA imaging.

B. *Introduction*

Carbon nanotubes (CNTs) represent a potentially powerful tool in cancer therapy and imaging. Previous studies have shown the possible applications of CNTs in photoacoustic and ultrasound imaging.[85,86] Photoacoustic (PA) and ultrasound (US) imaging are both powerful modalities but with considerable differences: (i) PA induces a tissue region to become an active acoustic source, while the conventional US introduces high-frequency acoustic waves and detects their echo; (ii) PA is broadband while US usually uses a single frequency. The former combines the advantages of both optical and ultrasonic imaging methods, and benefits from tissue's low acoustic scattering. Ultrasonic scattering in biological tissues is approximately three orders of magnitude less than optical scattering, enabling PA to achieve high acoustic resolution at depths much greater than the optical diffusion limit.[87,88] In addition, scattered light is less of an

issue to PA because any absorbed light is converted to sound. PA has also been shown to penetrate as deeply as 7 cm in tissue, which is adequate for many biomedical imaging applications.[89] On the other hand, despite the high potential of PA imaging, US imaging remains the most prevalent medical imaging modality due to cost of examination and safety.[90] Pure PA imaging typically also does not provide contextual anatomic information for effective localization of PA imaging signals *in vivo*.[91] Thus US-coregistered PA imaging has been reported to enable contextual anatomical information of PA signals.[92]

Previously, we created a novel formulation of highly dispersible CNTs that exhibit extremely high microwave heating capabilities, enabling the CNTs to be microwave thermal therapy transducers.[81] In order to evaluate the CNTs' ability to be delivered and tracked in real tissue, their ability to be imaged *in vivo* should be examined. In light of this, the present work was designed to test the CNTs in photoacoustic and ultrasound imaging focusing on the assessment and characterization of their NIR spectral and echogenic properties, as well as determining the distribution of CNTs *in vivo* following intratumoral injection.

C. *Research Design and Methods*

1. Preparation of CNT Dispersions

Previously synthesized CNTs were dispersed at 20 mg/ml in DI water with mannitol. The concentration of mannitol in DI water was ~50 mg/ml to achieve an osmolality within the range of blood (290-320 mOsm/kg); the osmolality was confirmed by a single-sample osmometer (Advanced Instruments 3D3). Control samples was prepared with DI water and mannitol only. All samples were sterilized via UV treatment for 30 min prior to *in vivo* studies.

2. Cell Culture

Human breast cancer cells (MCF7) were acquired from the American Type Culture Collection (ATCC) and maintained in RPMI medium from Life Technologies at standard incubation conditions (37°C, 5% CO_2). The cells were supplemented with 10% fetal bovine serum from Thermo Scientific and 1% penicillin-streptomycin from Life Technologies. All cells were cultured for up to 4 days before passaging, in which they will be pelleted by centrifugation at 1000 rpm for 5 minutes and resuspended in complete medium.

3. Xenograft Model

Immunodeficient male nu/nu mice (n = 2) at 43-56 days old from Charles River Laboratories were subcutaneously injected in both flanks with 10^6 MCF7 cells/100 µL under manual restraint. The injections were prepared by combining suspensions of 10^6 cells/50 µL cold 1x PBS with 50 µL Matrigel Basement Membrane Matrix from Corning. Mice were monitored weekly for tumor formation by caliper measurement until tumors reached ~200-250 mm^3 (2 weeks after injection). The tumor volumes were approximated according to the formula for an ellipsoid:[82,83]

$$volume = \frac{\pi * length * width * depth}{6}$$

All measurements were performed in triplicate. Animal imaging studies were performed by FUJIFILM VisualSonics.

4. Photoacoustic and Ultrasound Imaging

Echogenicity and US imaging of CNT samples were performed via a VisualSonics Vevo® 770 high-frequency ultrasound imaging system with a RMV707B 30 MHz probe operating in conventional ultrasound modality (B mode), depth 18 mm and 5 dB gain. To

exclude that possible air bubbles, present in the dispersions of the CNTs, might generate an echogenic signal, the samples were degassed prior to US imaging. The images were analyzed with the use of Adobe Photoshop CS5 software (Adobe Systems); the histograms of the frequency distribution of pixel echogenicity were determined according to a gray scale ranging from 0 (black) to 255 (white). US and PA images of tumors were taken using a co-registered real-time photoacoustic and ultrasound system with integrated fiber optics (LZ250, frequency = 21 MHz, wavelength = 800 nm, VisualSonics) with PA gain of 24 dB and B mode gain of 5 dB. Multispectral PA imaging was performed on CNT samples and methylene blue control across 680-970 nm wavelengths, along with longitudinal imaging at constant 815 nm. For all samples or tissues in US imaging, a thin layer of US gel was applied on the surface to reduce attenuation from any air pockets between the surfaces and probe, with the probe placed in direct contact with the gel. PA and US images obtained were analyzed using Vevo 2100 Workstation software (v1.4.0); tumor and injection volumes were calculated via manual fitting of a 3D contour in US images. The energies of the lasers used for imaging were all within the American National Standards Institute (ANSI) limitation (20 mJ/cm^2). For imaging studies, all mice were pre-anesthetized with isoflurane (5%) in O_2 mixture and maintained under 1–2.5% isoflurane; mice were placed on flat stationary surface and injection volumes of all samples were 10% of the estimated tumor volume.

5. Statistics

Data were analyzed from the average US signal from each CNT dispersion sample and average PA signal in each tumor. A two-sample t-Test was used to determine the significance of the difference in US signals between dispersion samples. A paired t-Test was used to determine

the significance of the difference in PA signals pre- and post-injection in the tumor tissue. Differences with $p < 0.05$ are considered significant.

D. Results

1. Echogenicity and Multispectral PA Characterization of CNTs

In order to characterize the echogenicity of the CNTs, we imaged samples of water + mannitol and CNT dispersions at different concentrations; the ultrasound images indicate a visible and strong ultrasound signal at the highest concentrations of the CNTs (2 and 20 mg/ml) and the intensity of the ultrasound signal was dose-dependent. We note that the dispersibility of the CNTs was previously shown to be persistent and stable for at least 3 months.[81] The US signal from dispersed CNTs at 2 mg/ml was approximately 3x more intense than water + mannitol as negative control (31.7 vs. 10.7, respectively; $P < 0.05$), whereas the US signal from dispersed CNTs at 20 mg/ml was more than 6x as intense as water + mannitol as negative control (68.7 vs. 10.7, respectively; $P < 0.05$) (Figure 18).
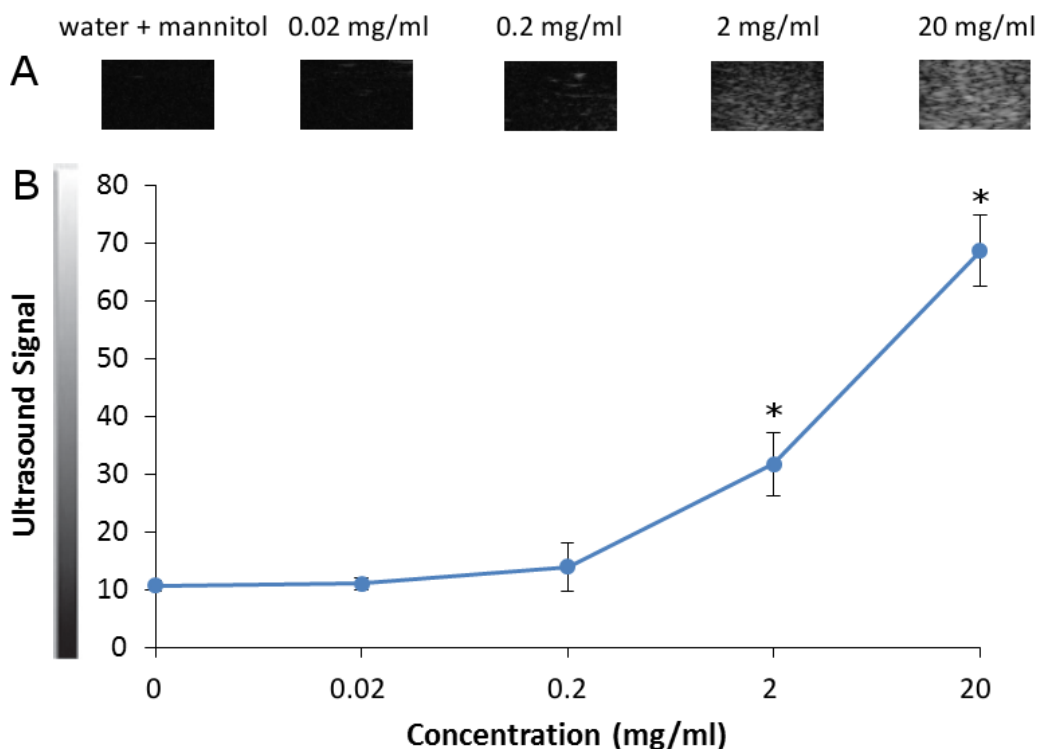
Figure 18: Ultrasound characterization of dispersed CNTs. (A) Representative ultrasound images of water + mannitol and CNTs (0.02-20 mg/ml). (B) Calculation of the ultrasound signal on different images (analyzed pixels = 6,400). The ultrasound signal is reported in 8-bit gray scale intensity from 0 to 255 shades of gray recordable. The error bars represent the SD (n = 6); *p < 0.05, compared to water + mannitol control.

In order to characterize the PA signal from the CNT dispersions, we performed both multispectral and longitudinal imaging (Figures 19A and 19B) of samples at NIR wavelengths. The multispectral absorption spectra (Figure 19C) demonstrate a relatively flat absorption spectrum for the CNT dispersions, with the spectrum consistent between the different concentrations. The results also demonstrate a very high NIR absorption and photoacoustic signal from the CNTs – at 680 nm, for example, the average PA signal of the 0.2 mg/ml and 2 mg/ml CNT dispersions (after subtracting signal from water + mannitol) was 2x (0.817) and 3x (1.166), respectively, that of methylene blue at 1/10 dilution (0.364). Longitudinal absorption spectra (Figure 19D) at 815 nm demonstrate a consistent PA signal across all imaging frames,

with an approximate 30% decrease in PA signal (1.22 to 0.89) between 20 and 2 mg/ml CNT samples.
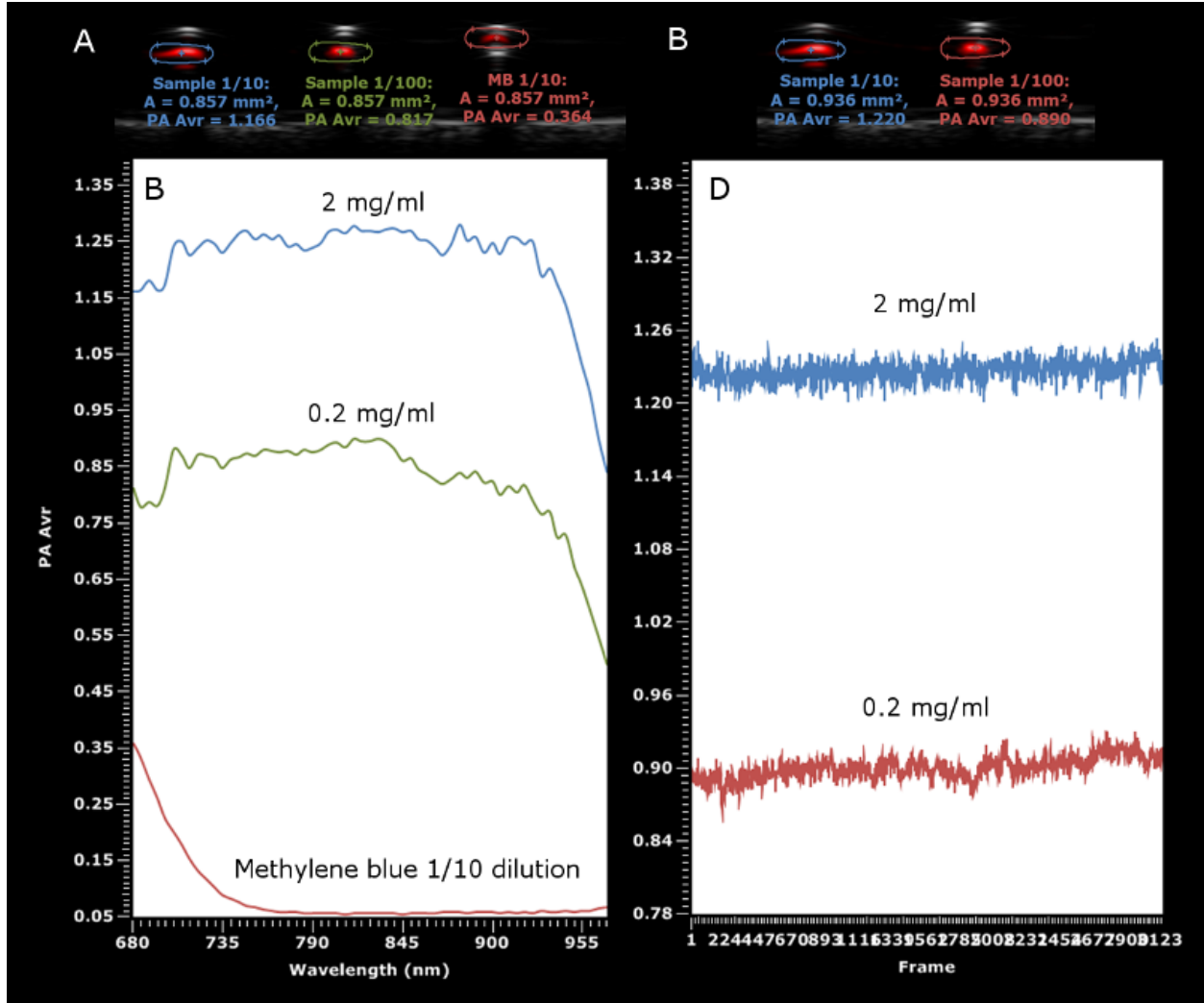
Figure 19: Photoacoustic imaging of CNT samples. (A) Multispectral imaging of CNT samples with 0.857 mm^2 analyzed image area for all samples. (B) Longitudinal photoacoustic imaging at 815 nm of CNT samples with 0.936 mm^2 analyzed image area for all samples. Signals from CNT samples were subtracted by signal from water + mannitol. *Raw data collected by Carly Warren.*

2. US and PA Imaging of Tumors

US-PA imaging of tumors pre- and post-injection of water + mannitol and CNT dispersions at 20 mg/ml were performed *in vivo*. Figure 20A shows representative US-coregistered PA images of tumors – regions pseudocolored in red are the PA signals next to

corresponding black and gray US images with the white arrows denoting higher contrast areas after injection of CNTs.
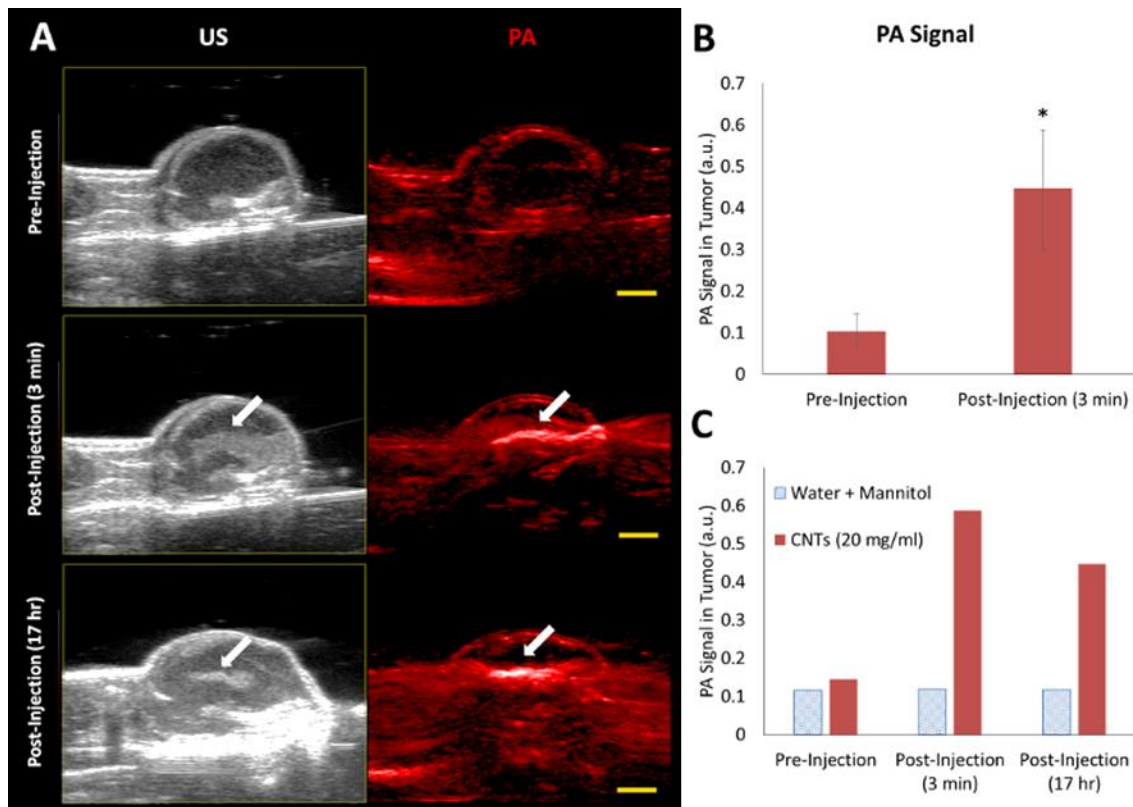
Figure 20: Ultrasound-photoacoustic images of tumors (A) pre- and post-injection of CNTs at 800 nm. White arrows denote areas of higher contrast from CNTs. Scale bar represents 3 mm. (B) Average PA signal in entire tumor pre- and post-injection of 20 mg/ml CNT dispersions at ~10% of tumor volumes. The error bars represent the min and max values (n = 3); *p < 0.05. (C) Longitudinal study of PA signal in one tumor sample pre- and post-injection. *Raw images collected by Carly Warren.*

The change in PA signal post-injection of CNTs into the tumors was greater than 4x (0.448 vs. 0.103, p < 0.05) (Figure 20B). In order to demonstrate the contribution to the PA signal from water + mannitol, we performed one control injection, which resulted in only a 3% increase in average PA signal within the tumor tissue. Furthermore, we performed longitudinal imaging in one of the CNT-injected tumors at 17 hours post-injection, yielding a relatively lower increase in PA signal (3x that of baseline) on average throughout the tumor.

Both the PA images in Figure 20 and changes in PA signal across different slices of the entire tumor (Figure 21) suggest that the distribution of CNTs appears to have consolidated to a narrower region within the tumor 17 hours post-injection compared to 3 min post-injection, leading to a relatively higher concentration of CNTs with fluid diffusion over time. These results confirm our histology results that demonstrate sequestration of CNTs within "pockets" of the solid tumor tissue at an approximate day post-injection.
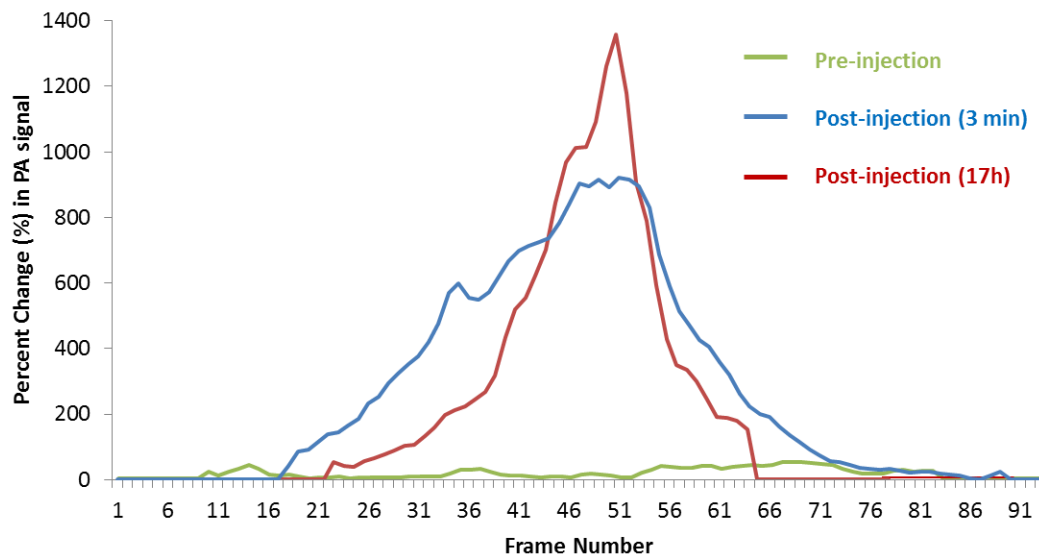
Figure 21: Change in PA signal by slice of tumor tissue from longitudinal PA imaging. *Raw data collected by Carly Warren.*

Using 3D contours, we quantified the volumes of both the tumors and injections (Figure 22) immediately following the injections. Based on the quantified volumes in the corresponding US images, the injected volumes reflected the estimated volumes injected manually via syringe (~10%). We note that even though both the tumor and injection volumes were quantified under US, contour estimates under PA images were similar 3 min post-injection.
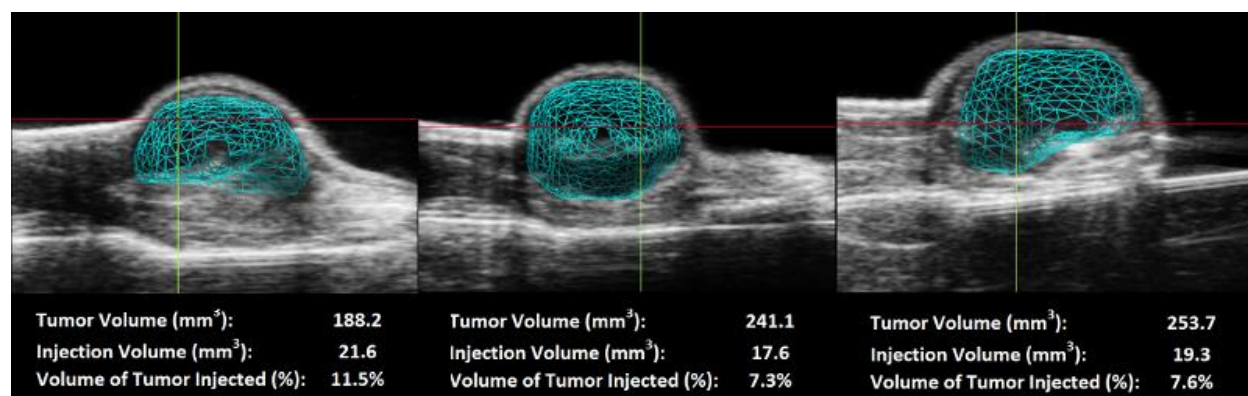
Figure 22: 3D contour fitting of ultrasound-photoacoustic images for volume calculation of tumors and CNT injections 10 min post-injection. *Raw images collected by Carly Warren.*

E. Discussion

In this study, we demonstrate that the CNT formulation under investigation can be imaged and quantified under US and PA imaging. The US signal from the dispersed CNTs was shown to be up to 6x as intense as water + mannitol as negative control at the highest concentration, whereas PA imaging demonstrated a robust signal from CNTs at relatively lower concentrations and longer times post-injection. The threshold for significant US signal from CNTs was 2 mg/ml compared to water-based control (Figure 18), whereas robust signal from CNTs were seen at much lower concentrations under PA imaging (Figure 19). Therefore, PA imaging appears to be a more quantitative modality in terms of assessing CNT concentrations and distributions *in vivo* than US imaging. We note that the epidermal layer produces PA signals due to presence of melanin and manifests as a continuous layer on the outside surface of the tumor.[93] In addition, other biomolecules such as hemoglobin also have significant absorbance at NIR wavelengths.[94] Since CNTs have a unique absorption spectrum and produce much stronger signals than those of melanin and hemoglobin,[85,95] the CNTs can easily be delineated and quantified from surrounding tissue with PA imaging.[96] These results demonstrate a promising proof-of-concept CNT platform that can be imaged under both US and PA imaging *in vivo*,

68

which enables non-invasive image-guided local delivery into target tissues under US imaging and non-invasive imaging and robust quantification post-injection under PA imaging. This has important implications for biomedical applications such as microwave hyperthermia and ablation since the CNT delivery and distribution need to be confirmed at least qualitatively before therapy in order to optimize therapeutic outcomes (i.e. maximize cancer tissue damage and minimize healthy tissue damage); moreover, a quantitative assessment of the distribution of CNTs within the tissue of interest is essential to determining parameters such as microwave power and timing of microwave irradiation during course of therapy, as well as the long-term biodistribution of the CNTs *in vivo*.

VII. Chapter 7: Summary and Future Work

A. *Summary*

This dissertation explores the development of a CNT platform for microwave hyperthermia applications that can be delivered safely into tumors and imaged *in vivo*. We piloted our investigations by establishing empirical evidence of SWCNTs enhancing the microwave dielectric properties of tissues *in vivo*. We also validated the need for local delivery strategies for adequate accumulation of CNTs into tumors for enhancement in microwave dielectric properties. With the preliminary assessments completed, we investigated the impact of acid sonication techniques on the microwave dielectric properties of CNT dispersions by characterizing the morphological and chemical changes across different CNT samples. Through this study, we identified the essential factors that have differential impact on the CNT's ability to enhance dielectric properties of the dispersion media. With the results in mind, we developed a formulation of CNTs with high dispersibility and microwave dielectric and heating properties by controlling the amount of sonication and functionalization in an acid bath – we noted that a key factor was an overall preservation of the chemical integrity of the CNTs. In order to demonstrate the feasibility of the CNTs as microwave hyperthermia agents *in vivo*, we injected the CNTs into tumors grown on mice and assessed their acute toxicity and ability to be imaged and monitored under both a conventional and novel imaging modality. The investigations heretofore demonstrate a proof-of-concept CNT platform that can serve as local microwave hyperthermia agents, is safe when injected in vivo and be tracked with different imaging modalities.

B. Future Work

In order to fully translate the CNT formulation under investigation into clinical applications involving microwave hyperthermia, the following future studies should be performed:

1. *In vivo* microwave hyperthermia efficacy studies

In order to demonstrate the feasibility of the CNT formulation to treat tumors, an *in vivo* study utilizing it along with microwave irradiation is required. With an *in vivo* tumor model, additional factors such as heat transfer and biological inflammatory response must also be considered with regards to ablation therapy. For example, how the CNTs conduct heat in tissue may change due to the so-called heat sink effect, in which the heat produced is dissipated and removed by increased blood flow.[97] Below is an outline of the experimental *in vivo* design.

Experimental variables: Effect of the microwave irradiation and existence of CNTs will be examined on the tumor-bearing mice. Tumor size and mouse survival rate will be measured.

Experimental design: The preparation of the CNT dispersions, cell culture and xenograft model should be similar to protocols delineated in [Chapter 5]'s acute toxicity study. In brief, immunodeficient nude mice at 43-56 days old will be subcutaneously injected in the right flanks with MCF7 cells. Animal groups are summarized in Table VI.

Table VI. Study design for *in vivo* hyperthermia

Group	Dose	# Animals
Sham Control	-	6
Sham Control + Treatment	-	6
Vehicle Control	10% tumor volume	6
Vehicle Control + Treatment	10% tumor volume	6
CNTs + Vehicle	10% tumor volume; 2 mg/cm^3 in tumor	6
CNTs + Vehicle + Treatment	10% tumor volume; 2 mg/cm^3 in tumor	6

Based on Figure 10 [Chapter 4], 20 mg/ml CNTs + mannitol could be used to induce heating above 43 ºC within 1 minute under a microwave (3GHz, 1W) amplifier and synthesizer system. Microwave irradiation to the injection group will be applied at 3 min post-injection into the tumors and hyperthermia (>43 ºC) will be induced and maintained in the tumors for 10 min. Surface temperatures of the subcutaneous tumor will be monitored in real-time during microwave irradiation using an infrared camera. In order to monitor the temperature of collateral tissue underneath the tumors, fiber-optic temperature probes connected to a fluoroptic thermometer will be needle-guided and placed under the tumor site. At the conclusion of the hyperthermia treatments, the mice and tumor sizes will be monitored for 14 days until tumor extraction. Tumor volumes will be monitored every 2 days for 14 days and mice survival data will be collected. According to animal care and use regulations, mice with tumor diameters greater than 15 mm or if sick will be euthanized.

Data analysis and interpretation: Effective ablation therapy will be confirmed if the microwave-irradiated group with CNTs has a statistically significant change in tumor size over the other groups. A one-way ANOVA analysis will be performed to compare tumor volumes for

each group and survival data will be compared using the Kaplan-Meier method. As presented in [Chapter 5], there was no statistically significant change in tumor size at 14 days from the presence of CNTs alone in the tumor.

Limitations: A major limitation of this study is the inability to monitor effects at the cellular and molecular level after microwave irradiation, as the study is focused on tumor sizing and survival rate outcomes. Moreover, possible skin burning and scarring can also significantly impact tumor monitoring. Thus if the effects of the microwave ablation are significant, histological analyses should be performed at various time-points (e.g. 1 and 14 days post-treatment). Another limitation of this study may be the variation across temperature changes due to an irregular distribution of CNTs within the tumor. To address this, samples with large variations in temperatures should be excluded from analysis. However, this may lead to a need for larger sample sizes. To reduce this need, computational modeling of heat transport can help eliminate additional parameters, such as microwave power.

2. Cell studies

Although the results of the acute toxicity studies [Chapter 5] did not show a significant difference in tumor volumes between CNT-injected and control groups at Day 14, Figure 15 suggests a trend towards minor inhibition of tumor growth following injection of the CNTs. Whether or not this trend is due to CNT uptake by cells or physical inhibitions via displacement of extracellular matrices is undetermined – indeed, histology results are unable to determine whether CNTs are inside or on the surface of the cells in the vicinity. Thus, *in vitro* studies with cells incubated with CNTs will be performed to investigate whether the tumor cells uptake the CNTs, and whether there is a dose-dependent toxicity.

Experimental variables: Cytotoxicity will be assessed with assay chemicals. Uptake will be assessed by high-resolution imaging.

Experimental design: The cancer cell line will be MCF7 breast cancer cells. Since these are epithelial cancer cells, the near proximity of skin warrants the inclusion of a fibroblast cell line (3T3) to be included as a healthy cell reference. Cytotoxicity studies will be performed at different CNT concentrations. Previous reports have shown that many common assays give false positive results because the assay chemicals absorb on the CNTs and cannot perform their necessary enzymatic reactions for an accurate reading.[98] In addition, the presence of CNTs within the solution can interfere with signal readout, such as colorimetric or fluorometric signals, due to the broad absorbance of CNTs within the entire visible and NIR spectrum. Thus a modified lactate dehydrogenase (LDH) assay that eliminates the interaction between the enzymatic reactions required for LDH detection will be used to reduce interference and false results.[99] The concentrations of CNTs assessed will be relevant to the doses injected *in vivo* [Chapter 5 and 6] – the equivalent of 2 mg/cm^3 of tumor. For a mid-point concentration reference, we would consider the situation in which the mass of CNTs injected is exposed uniformly to all cells in the volume. According to a previous study, epithelial tumors hold on the order of 10^8 cells per cm^3 or per g.[100] Thus, as an estimation, a 24-well plate with a 60-80% confluent density of 0.2 x 10^6 cells and 500 µl plating medium would require a mid-point CNT concentration of:

$$2\frac{mg}{cm^3} \ x \ \frac{1000\ \mu g}{mg} \ x \frac{cm^3}{10^8\ cells} \ x \frac{0.2x10^6 cells}{500\ \mu l} \ x \frac{1000\ \mu l}{ml} = \boldsymbol{8\frac{\mu g}{ml}}$$

With this in mind, the concentrations will be varied on a logarithmic scale (0, 0.8, 8, 80 and 800 µg/ml). In order to determine whether CNTs are being uptaken by cells, imaging will be

performed with either cryo-transmission electron microscopy (TEM) or z-profile signals from confocal Raman microspectroscopy.

Data analysis and interpretation: All cytotoxicity measurements will be performed in pentaplicate and analyzed via one-way ANOVA for statistical significance. Z-profile signals between CH_2 and G band Raman signal area-under-the-curves (AUCs) will be correlated by Pearson's product-moment correlation. TEM images will provide qualitative assessments of CNT uptake into cells.

Limitations: A major limitation of this study is the discrepancy between modeling CNT exposure *in vitro* to represent *in vivo* studies. Our mid-point concentration estimate is based on the assumption that the CNTs would be exposed uniformly to all cells *in vivo*, which is not the case with the heterogeneous tissue distribution from localized delivery of CNTs. Therefore, any dose-dependent toxicity results *in vitro* does not necessarily translate to any relevant doses *in vivo*. Furthermore, if cellular uptake is observed along with apparent toxicity, we cannot preclude the possibility of an indirect toxicity effect from micronutrients in the medium being adsorbed onto CNTs.[84] We can determine whether CNTs adsorb micronutrients by running adsorption isotherms, in which CNTs are added to solute solutions (phenol red, tyrosine or folic acid), mixed, centrifuged and then filtered out. The changes in optical absorbance of the supernatants will be measured with a UV/Vis spectrometer at 560 (phenol red), 280 (tyrosine), and 350 (folate) nm. For amino acid and vitamins, the same procedure will apply but samples will be analyzed by high-performance liquid chromatography (HPLC) using UV, fluorescence and tandem mass spectrometry.

3. Biodistribution and long-term fate of CNTs *in vivo*

Histological results from the acute toxicity studies described in Chapter 5 did not show any obvious accumulation of CNTs in essential organs following intra-tumoral injections of the CNTs. However, long-term studies of the CNTs' activity are necessary to understand their overall biodistribution whether given systemic exposure or not. These studies would have to be performed in non-tumor bearing mice models, such as Balb/c mice, to avert early mortality due to continued tumor growth. Alternatively, if the study is to be coupled with a different tumor model, such as hepatic cancer, suitable animal models such as rabbits may be used. Important questions include: 1) how long do the CNTs remain in the body and how do they accumulate in different organs depending on the particular injection method (as outlined in [Chapter 1], there are many different methods of local injections depending on the target tissue, which ultimately is dependent on the cancer model being investigated), 2) what is the blood circulation half-life of CNTs, and 3) what is the clearance pathway?

Given long-term distribution studies lasting on the order of months, techniques such as PET imaging that utilize conjugated radiolabels, such as [125]I (60-day half-life) can be used, although this requires expensive precautions during animal experiments. Previous studies have also used Raman spectroscopy and PA to monitor and image, respectively, CNTs in excised organs.[101] These modalities directly detect the intrinsic properties of the CNTs (as discussed in Chapter 13 and Chapter 6), rather than labels that may disassociate or degrade over time *in vivo*. Furthermore, the Raman G-band peak can quantitatively correlate the CNT concentration when measured in tissue lysate or buffer.[101]

The proposed long-term biodistribution study will also include monitoring of potential systemic toxicities associated with CNT exposure compared to control animals by monitoring

mortality rates, body weights and a serum chemistry panel on collected blood samples. Blood will be collected at pre-specified time-points and/or after euthanasia and analyzed for serum proteins, which would reveal any metabolic changes following CNT injections. Serum chemistry will include a panel of markers, such as albumin, cholesterol, and glucose.

Experimental variables: Raman and PA imaging of excised organs and blood of animals will be collected. The Raman G-band and PA signal intensity will be correlated with CNT concentration and monitored over time. The CNT %ID/g of all major organs post-injection will be measured. Blood, urine and feces collected at different time-points will be used to measure serum levels, circulation half-life, excretion rates and CNT concentration changes over time. Mortality rates and body weight changes will also be monitored.

Experimental design: Biodistribution studies will be performed on animals for up to 5 months post-injection of CNTs, with n = 5. Sacrifices will be made at incremental time-points (e.g. 0, 1, 15, 30, 60, 90, 120, 150 days) and all major organs will be excised and weighed; blood samples will also be collected. PA and Raman imaging of organ samples will be performed – samples will be lysed into a buffer solution consisting of sodium dodecyl sulfate (SDS), Triton, and dithiothreitol (DTT) and homogenized via sonication; the lysate will then be heated to obtain a clear homogenate.[101] A calibration curve of Raman G-band and PA signal intensity and AUC measurements vs. CNT concentration will be collected under same imaging conditions (wavelength, power, spot size and collection time). Once the concentration of CNTs is correlated with the calibration curve, the %ID/g will be calculated for each organ at each time point. A serum chemistry panel consisting of albumin, cholesterol and glucose markers will be collected and circulation half-life of CNTs will be calculated from blood sampling. Urine and feces will be collected and body weights at each time point will be recorded.

Data analysis and interpretation: The long-term amounts of CNTs in all major organs will be the key output of this study. The rate of CNT concentration decrease and analyses of urine and feces will allow for hypothesizing the excretion pathway (i.e. liver biliary ducts, intestines, renal excretion, reticuloendothelial system, etc.). If clearance of CNTs from major organs do not occur after a long period (e.g. 3 months), toxicity would likely be expected. This would be corroborate by body weight loss, increased mortality rates and/or significantly different serum chemistry from the CNT-injected group over control group.

Limitations: One of the biggest limitations lies in the sensitivity of Raman and PA imaging to the concentration of CNTs. It may be likely that CNT concentrations may not be detectable by either detection method, particularly at later time-points. This limit of detection will be established from calibration curves of Raman G-band and PA intensities vs. CNT concentration. In order to be able to establish a pattern of clearance, a high and low (one in which toxicity is not expected) dose of CNTs will be injected. Toxicity will be characterized by serum markers and histological analyses can reveal additional qualitative measures. Specifically, histology can be performed with H&E staining and with terminal deoxynucleotidy transferase biotin-dUTP nick-end labeling (TUNEL) to detect DNA damage due to apoptosis or necrosis.

4. Future of carbon nanotubes

To realize the full potential of utilizing the unique properties of carbon nanotubes, such as high thermal conductivity, permittivity and intrinsic optical signals, high-level purity and uniformity will be required. One of the most important tasks taken up by the National Institute of Standards and Technology (NIST) is to separate CNTs by their electronic and morphological properties. Scaling up and commercializing laboratory-developed separation techniques, such as density gradient ultracentrifugation or column purification, will be essential for this task. An

increased confidence in the purity of CNTs, and separation based on essential differences such as semiconducting vs. metallic CNTs will allow researchers to better develop CNTs for biomedical applications. Properties such as length and functionalization are particularly important when considering biological interaction with CNTs. Even though there are many studies on different types of carbon-based nanoparticles, comparison across studies is very limited due to the non-uniform nature of the nanoparticles in different studies; this is further compounded by differences in concentration, functionalization method and *in vivo* animal model. Standardizing a reference material for CNTs will greatly advance their potential for biomedical applications.

REFERENCES

1.   Chu KF and Dupuy DE. Thermal ablation of tumours: biological mechanisms and advances in therapy. *Nature Reviews Cancer*. 2014; 14: 199-208.

2.   Alberts B, Johnson A, Lewis J, Raff M, Roberts K and Walter P. Cancer Treatment: Present and Future. 2002.

3.   Repasky EA, Evans SS and Dewhirst MW. Temperature matters! And why it should matter to tumor immunologists. *Cancer immunology research*. 2013; 1: 210-6.

4.   Zhang H-G, Mehta K, Cohen P and Guha C. Hyperthermia on immune regulation: a temperature's story. *Cancer letters*. 2008; 271: 191-204.

5.   Chicheł A, Skowronek J, Kubaszewska M and Kanikowski M. Hyperthermia–description of a method and a review of clinical applications. *Reports of Practical Oncology & Radiotherapy*. 2007; 12: 267-75.

6.   IP Soares P, MM Ferreira I, AGBN Igreja R, MM Novo C and PMR Borges J. Application of hyperthermia for cancer treatment: recent patents review. *Recent patents on anti-cancer drug discovery*. 2012; 7: 64-73.

7.   Sanchez-Ortiz RF, Tannir N, Ahrar K and Wood CG. Spontaneous regression of pulmonary metastases from renal cell carcinoma after radio frequency ablation of primary tumor: in situ tumor vaccine? *The Journal of urology*. 2003; 170: 178-9.

8.   Kim H, Park BK and Kim CK. Spontaneous regression of pulmonary and adrenal metastases following percutaneous radiofrequency ablation of a recurrent renal cell carcinoma. *Korean journal of radiology*. 2008; 9: 470-2.

9.   Soanes W, Ablin R and Gonder M. Remission of metastatic lesions following cryosurgery in prostatic cancer: immunologic considerations. *The Journal of urology*. 1970; 104: 154-9.

10.   Machlenkin A, Goldberger O, Tirosh B, et al. Combined dendritic cell cryotherapy of tumor induces systemic antimetastatic immunity. *Clinical cancer research*. 2005; 11: 4955-61.

11.   Urano M, Tanaka C, Sugiyama Y, Miya K and Saji S. Antitumor effects of residual tumor after cryoablation: the combined effect of residual tumor and a protein-bound polysaccharide on multiple liver metastases in a murine model. *Cryobiology*. 2003; 46: 238-45.

12.   den Brok MH, Sutmuller RP, Nierkens S, et al. Synergy between in situ cryoablation and TLR9 stimulation results in a highly effective in vivo dendritic cell vaccine. *Cancer research*. 2006; 66: 7285-92.

13.   Fornage BD and Hwang RF. Current status of imaging-guided percutaneous ablation of breast cancer. *American Journal of Roentgenology*. 2014; 203: 442-8.

14.   Bai J, Liu P and Xu L. Recent advances in thermal treatment techniques and thermally induced immune responses against cancer. *IEEE Transactions on Biomedical Engineering*. 2014; 61: 1497-505.

15.   Bleaney BI, Bleaney BI and Bleaney B. *Electricity and Magnetism, Volume 2*. Oxford University Press, 2013.

16.   Shea JD, Veen BDV and Hagness SC. A TSVD Analysis of Microwave Inverse Scattering for Breast Imaging. *IEEE Transactions on Biomedical Engineering*. 2012; 59: 936-45.

17.   John H, Lienhard I, John H and Lienhard V. A heat transfer textbook. *Phlogiston Press, Cambridge*. 2008.

18.   Liu Z, Tabakman S, Welsher K and Dai H. Carbon nanotubes in biology and medicine: In vitro and in vivo detection, imaging and drug delivery. *Nano Research*. 2009; 2: 85-120.

19.   Shea J, Kosmas P, Van Veen B and Hagness S. Contrast-enhanced microwave imaging of breast tumors: a computational study using 3D realistic numerical phantoms. *Inverse Problems*. 2010; 26: 074009.

20.   Young JK, Figueroa ER and Drezek RA. Tunable nanostructures as photothermal theranostic agents. *Annals of biomedical engineering*. 2012; 40: 438-59.

21.   Gannon CJ, Cherukuri P, Yakobson BI, et al. Carbon nanotube-enhanced thermal destruction of cancer cells in a noninvasive radiofrequency field. *Cancer*. 2007; 110: 2654-65.

22.   Mashal A, Sitharaman B, Li X, et al. Toward carbon-nanotube-based theranostic agents for microwave detection and treatment of breast cancer: enhanced dielectric and heating response of tissue-mimicking materials. *IEEE Trans Biomed Eng*. 2010; 57: 1831-4. Epub 2010 Feb 18.

23.   Li X, Sahakian AV, Messersmith P, Hagness SC, Booske JH and Knezevic I. Nanoparticle Contrast Agents for Enhanced Microwave Imaging and Thermal Treatment of Breast Cancer. DTIC Document, 2010.

24.   Mashal A, Booske JH and Hagness SC. Toward contrast-enhanced microwave-induced thermoacoustic imaging of breast cancer: an experimental study of the effects of microbubbles on simple thermoacoustic targets. *Physics in medicine and biology*. 2009; 54: 641.

25.   Mashal A, Sitharaman B, Li X, et al. Toward carbon-nanotube-based theranostic agents for microwave detection and treatment of breast cancer: enhanced dielectric and heating response of tissue-mimicking materials. *IEEE Transactions on Biomedical Engineering*. 2010; 57: 1831-4.

26.   Popovic D, McCartney L, Beasley C, et al. Precision open-ended coaxial probes for in vivo and. ex vivo dielectric spectroscopy of biological tissues at microwave, frequencies. *IEEE Trans Microw Theory Tech*. 2005; 53: 1713-22.

27.   Gao F, Hagness SC, Booske JH, Xie SX and Sitharaman B. In vivo microwave dielectric spectroscopy of breast tumor xenografts with intra-tumoral injections of SWCNT dispersions. *Instrumentation and Measurement Technology Conference (I2MTC), 2013 IEEE International*. IEEE, 2013, p. 1441-4.

28.   Lazebnik M, Popovic D, McCartney L, et al. A large-scale study of the ultrawideband microwave dielectric properties of normal, benign and malignant breast tissues obtained from cancer surgeries. *Physics in Medicine and Biology*. 2007; 52: 6093.

29.   Bae YH and Park K. Targeted drug delivery to tumors: myths, reality and possibility. *Journal of controlled release*. 2011; 153: 198.

30.   Tasis D, Tagmatarchis N, Bianco A and Prato M. Chemistry of carbon nanotubes. *Chem Rev*. 2006; 106: 1105-36.

31.   Harrison BS and Atala A. Carbon nanotube applications for tissue engineering. *Biomaterials*. 2007; 28: 344-53.

32.   De La Zerda A, Zavaleta C, Keren S, et al. Carbon nanotubes as photoacoustic molecular imaging agents in living mice. *Nat Nano*. 2008; 3: 557-62.

33.   Liu Z, Tabakman S, Welsher K and Dai H. Carbon Nanotubes in Biology and Medicine: In vitro and in vivo Detection, Imaging and Drug Delivery. *Nano Res*. 2009; 2: 85-120.

34.   McDevitt MR, Chattopadhyay D, Kappel BJ, et al. Tumor Targeting with Antibody-Functionalized, Radiolabeled Carbon Nanotubes. *Journal of Nuclear Medicine*. 2007; 48: 1180-9.

35.   Ruggiero A, Villa CH, Holland JP, et al. Imaging and treating tumor vasculature with targeted radiolabeled carbon nanotubes. *International journal of nanomedicine*. 2010; 5: 783.

36.   Liu Z, Cai W, He L, et al. In vivo biodistribution and highly efficient tumour targeting of carbon nanotubes in mice. *Nat Nano*. 2007; 2: 47-52.

37.   Grimm J and Scheinberg DA. Will nanotechnology influence targeted cancer therapy? *Seminars in radiation oncology*. Elsevier, 2011, p. 80-7.

38.   Xie SX, Gao F, Patel SC, Booske JH, Hagness SC and Sitharaman B. Effect of synthesis and acid purification methods on the microwave dielectric properties of single-walled carbon nanotube aqueous dispersions. *Applied Physics Letters*. 2013; 103: 133114.

39.   Mouli SK, Tyler P, McDevitt JL, et al. Image-Guided Local Delivery Strategies Enhance Therapeutic Nanoparticle Uptake in Solid Tumors. *ACS Nano*. 2013; 7: 7724-33.

40.   Hou P-X, Liu C and Cheng H-M. Purification of carbon nanotubes. *Carbon*. 2008; 46: 2003-25.

41.   Peng H, Alemany LB, Margrave JL and Khabashesku VN. Sidewall Carboxylic Acid Functionalization of Single-Walled Carbon Nanotubes. *Journal of the American Chemical Society*. 2003; 125: 15174-82.

42.   Mackeyev Y, Bachilo S, Hartman KB and Wilson LJ. The purification of HiPco SWCNTs with liquid bromine at room temperature. *Carbon*. 2007; 45: 1013-7.

43.   Hersam MC. Progress towards monodisperse single-walled carbon nanotubes. *Nature Nanotechnology*. 2008; 3: 387-94.

44.   Wang Y, Kim MJ, Shan H, et al. Continued Growth of Single-Walled Carbon Nanotubes. *Nano Letters*. 2005; 5: 997-1002.

45.   Mansfield E, Kar A and Hooker SA. Applications of TGA in quality control of SWCNTs. *Analytical & Bioanalytical Chemistry*. 2010; 396: 1071-7.

46.   Wang, Shan H, Hauge RH, Pasquali M and Smalley RE. A Highly Selective, One-Pot Purification Method for Single-Walled Carbon Nanotubes. *The Journal of Physical Chemistry B*. 2007; 111: 1249-52.

47.   Hu H, Zhao B, Itkis ME and Haddon RC. Nitric Acid Purification of Single-Walled Carbon Nanotubes. *The Journal of Physical Chemistry B*. 2003; 107: 13838-42.

48.   Li WZ, Wen JG, Sennett M and Ren ZF. Clean double-walled carbon nanotubes synthesized by CVD. *Chemical Physics Letters*. 2003; 368: 299-306.

49.   Jung YC, Shimamoto D, Muramatsu H, et al. Robust, Conducting, and Transparent Polymer Composites Using Surface-Modified and Individualized Double-Walled Carbon Nanotubes. *Advanced Materials*. 2008; 20: 4509-12.

50.   Eklund PC, Holden JM and Jishi RA. Vibrational modes of carbon nanotubes; Spectroscopy and theory. *Carbon*. 1995; 33: 959-72.

51.   Hussain S, Jha P, Chouksey A, et al. Spectroscopic Investigation of Modified Single Wall Carbon Nanotube (SWCNT). *Journal of Modern Physics*. 2011; 2: 538-43.

52.   Zhou W, Ooi YH, Russo R, et al. Structural characterization and diameter-dependent oxidative stability of single wall carbon nanotubes synthesized by the catalytic decomposition of CO. *Chemical Physics Letters*. 2001; 350: 6-14.

53.   Tchoul MN, Ford WT, Lolli G, Resasco DE and Arepalli S. Effect of Mild Nitric Acid Oxidation on Dispersability, Size, and Structure of Single-Walled Carbon Nanotubes. *Chemistry of Materials*. 2007; 19: 5765-72.

54.   Rinzler AG, Liu J, Dai H, et al. Large-scale purification of single-wall carbon nanotubes: process, product, and characterization. *Appl Phys A*. 1998; 67: 29-37.

55.   Dillon AC, Gennett T, Jones KM, Alleman JL, Parilla PA and Heben MJ. A Simple and Complete Purification of Single-Walled Carbon Nanotube Materials. *Advanced Materials*. 1999; 11: 1354-8.

56.   Brown SDM, Jorio A, Corio P, et al. Origin of the Breit-Wigner-Fano lineshape of the tangential G-band feature of metallic carbon nanotubes. *Physical Review B*. 2001; 63: 155414.

57.   Ren W, Li F, Chen J, Bai S and Cheng H-M. Morphology, diameter distribution and Raman scattering measurements of double-walled carbon nanotubes synthesized by catalytic decomposition of methane. *Chemical Physics Letters*. 2002; 359: 196-202.

58.   Shi Z, Lian Y, Liao F, et al. Purification of single-wall carbon nanotubes. *Solid State Communications*. 1999; 112: 35-7.

59.   Smart SK, Ren WC, Cheng HM, Lu GQ and Martin DJ. Shortened double-walled carbon nanotubes by high-energy ball milling. *International Journal of Nanotechnology*. 2007; 4: 618-33.

60.   Brukh R, Sae-Khow O and Mitra S. Stabilizing single-walled carbon nanotubes by removal of residual metal catalysts. *Chemical Physics Letters*. 2008; 459: 149-52.

61.   Avti PK, Talukdar Y, Sirotkin MV, Shroyer KR and Sitharaman B. Toward single-walled carbon nanotube–gadolinium complex as advanced MRI contrast agents: Pharmacodynamics and global genomic response in small animals. *Journal of Biomedical Materials Research Part B: Applied Biomaterials*. 2013; 101B: 1039-49.

62.   Adminstration USFaD.

63.   Lin Y, Allard LF and Sun Y-P. Protein-affinity of single-walled carbon nanotubes in water. *The Journal of Physical Chemistry B*. 2004; 108: 3760-4.

64.   Jeynes JCG, Mendoza E, Chow DC, Watts PC, McFadden J and Silva SRP. Generation of Chemically Unmodified Pure Single-Walled Carbon Nanotubes by Solubilizing with RNA and Treatment with Ribonuclease A. *Advanced Materials*. 2006; 18: 1598-602.

65.   Datsyuk V, Kalyva M, Papagelis K, et al. Chemical oxidation of multiwalled carbon nanotubes. *Carbon*. 2008; 46: 833-40.

66.   Wang Y, Iqbal Z and Mitra S. Rapidly functionalized, water-dispersed carbon nanotubes at high concentration. *Journal of the American Chemical Society*. 2006; 128: 95-9.

67.   Li Y, Zhang X, Luo J, et al. Purification of CVD synthesized single-wall carbon nanotubes by different acid oxidation treatments. *Nanotechnology*. 2004; 15: 1645.

68.   Xie S, Gao F, Patel S, Booske J, Hagness S and Sitharaman B. Clinically Relevant CNT Dispersions with Exceptionally High Dielectric Properties for Microwave Theranostic Applications.

69.   Li W, Wen J, Sennett M and Ren Z. Clean double-walled carbon nanotubes synthesized by CVD. *Chemical Physics Letters*. 2003; 368: 299-306.

70.   Jung YC, Shimamoto D, Muramatsu H, et al. Robust, Conducting, and Transparent Polymer Composites Using Surface-Modified and Individualized Double-Walled Carbon Nanotubes. *Advanced Materials*. 2008; 20: 4509-12.

71.   Shen C, Brozena AH and Wang Y. Double-walled carbon nanotubes: Challenges and opportunities. *Nanoscale*. 2011; 3: 503-18.

72.   Nagasawa S, Yudasaka M, Hirahara K, Ichihashi T and Iijima S. Effect of oxidation on single-wall carbon nanotubes. *Chemical Physics Letters*. 2000; 328: 374-80.

73.   Kastner J, Pichler T, Kuzmany H, et al. Resonance Raman and infrared spectroscopy of carbon nanotubes. *Chemical Physics Letters*. 1994; 221: 53-8.

74.	Mawhinney DB, Naumenko V, Kuznetsova A, Yates Jr JT, Liu J and Smalley R. Surface defect site density on single walled carbon nanotubes by titration. *Chemical Physics Letters*. 2000; 324: 213-6.

75.	Pradhan BK and Sandle N. Effect of different oxidizing agent treatments on the surface properties of activated carbons. *Carbon*. 1999; 37: 1323-32.

76.	Stobinski L, Lesiak B, Kövér L, et al. Multiwall carbon nanotubes purification and oxidation by nitric acid studied by the FTIR and electron spectroscopy methods. *Journal of Alloys and Compounds*. 2010; 501: 77-84.

77.	Kostarelos K. The long and short of carbon nanotube toxicity. *Nature biotechnology*. 2008; 26: 774-6.

78.	Heister E, Lamprecht C, Neves V, et al. Higher dispersion efficacy of functionalized carbon nanotubes in chemical and biological environments. *ACS Nano*. 2010; 4: 2615-26.

79.	Hobbs SK, Monsky WL, Yuan F, et al. Regulation of transport pathways in tumor vessels: role of tumor type and microenvironment. *Proceedings of the National Academy of Sciences*. 1998; 95: 4607-12.

80.	Gao F, Hagness SC, Booske JH, Xie SX and Sitharaman B. In vivo microwave dielectric spectroscopy of breast tumor xenografts with intra-tumoral injections of SWCNT dispersions. *2013 IEEE International Instrumentation and Measurement Technology Conference (I2MTC)*. IEEE, 2013, p. 1441-4.

81.	Xie SX, Gao F, Patel SC, Booske JH, Hagness SC and Sitharaman B. Clinically relevant CNT dispersions with exceptionally high dielectric properties for microwave theranostic applications. *IEEE Transactions on Biomedical Engineering*. 2014; 61: 2718-23.

82.	Giustini AJ, Petryk AA and Hoopes PJ. Comparison of microwave and magnetic nanoparticle hyperthermia radiosensitization in murine breast tumors. *SPIE BiOS*. International Society for Optics and Photonics, 2011, p. 79010E-E-7.

83.	Raoof M, Corr SJ, Zhu C, et al. Gold nanoparticles and radiofrequency in experimental models for hepatocellular carcinoma. *Nanomedicine: Nanotechnology, Biology and Medicine*. 2014.

84.	Guo L, Von Dem Bussche A, Buechner M, Yan A, Kane AB and Hurt RH. Adsorption of essential micronutrients by carbon nanotubes and the implications for nanotoxicity testing. *Small*. 2008; 4: 721-7.

85.	De La Zerda A, Zavaleta C, Keren S, et al. Carbon nanotubes as photoacoustic molecular imaging agents in living mice. *Nature nanotechnology*. 2008; 3: 557-62.

86.	Delogu LG, Vidili G, Venturelli E, et al. Functionalized multiwalled carbon nanotubes as ultrasound contrast agents. *Proceedings of the National Academy of Sciences*. 2012; 109: 16612-7.

87.	Wang LV. Multiscale photoacoustic microscopy and computed tomography. *Nature photonics*. 2009; 3: 503-9.

88.	Oraevsky A and Karabutov A. Optoacoustic tomography. *Biomedical photonics handbook*. 2003; 34: 1-34.

89.	Ke H, Erpelding TN, Jankovic L, Liu C and Wang LV. Performance characterization of an integrated ultrasound, photoacoustic, and thermoacoustic imaging system. *Journal of biomedical optics*. 2012; 17: 0560101-6.

90.	Postema M and Gilja OH. Contrast-enhanced and targeted ultrasound. *World J Gastroenterol*. 2011; 17: 28-41.

91.   Emelianov SY, Li P-C and O'Donnell M. Photoacoustics for molecular imaging and therapy. *Physics today*. 2009; 62: 34.

92.   Aguirre A, Guo P, Gamelin J, et al. Coregistered three-dimensional ultrasound and photoacoustic imaging system for ovarian tissue characterization. *Journal of biomedical optics*. 2009; 14: 054014--9.

93.   Viator JA, Komadina J, Svaasand LO, Aguilar G, Choi B and Nelson JS. A comparative study of photoacoustic and reflectance methods for determination of epidermal melanin content. *Journal of investigative dermatology*. 2004; 122: 1432-9.

94.   Edwards A, Richardson C, Van Der Zee P, et al. Measurement of hemoglobin flow and blood flow by near-infrared spectroscopy. *Journal of Applied Physiology*. 1993; 75: 1884-9.

95.   Pramanik M, Song KH, Swierczewska M, Green D, Sitharaman B and Wang LV. In vivo carbon nanotube-enhanced non-invasive photoacoustic mapping of the sentinel lymph node. *Physics in medicine and biology*. 2009; 54: 3291.

96.   Avti PK, Hu S, Favazza C, et al. Detection, mapping, and quantification of single walled carbon nanotubes in histological specimens with photoacoustic microscopy. *PloS one*. 2012; 7: e35064.

97.   Lu DS, Raman SS, Vodopich DJ, Wang M, Sayre J and Lassman C. Effect of vessel size on creation of hepatic radiofrequency lesions in pigs: assessment of the "heat sink" effect. *American Journal of Roentgenology*. 2002; 178: 47-51.

98.   Wörle-Knirsch J, Pulskamp K and Krug H. Oops they did it again! Carbon nanotubes hoax scientists in viability assays. *Nano letters*. 2006; 6: 1261-8.

99.   Grosseau JP. Adsorption of lactate dehydrogenase enzyme on carbon nanotubes: how to get accurate results about the cytotoxicity of these nanomaterials.

100.   Del Monte U. Does the cell number 109 still really fit one gram of tumor tissue? *Cell Cycle*. 2009; 8: 505-6.

101.   Liu Z, Davis C, Cai W, He L, Chen X and Dai H. Circulation and long-term fate of functionalized, biocompatible single-walled carbon nanotubes in mice probed by Raman spectroscopy. *Proceedings of the National Academy of Sciences*. 2008; 105: 1410-5.